



The evolution of a mid-crustal thermal aureole at Cerro Toro, Sierra de Famatina, NW Argentina



P.H. Alasino^{a,b,*}, C. Casquet^c, M.A. Larrovere^{a,b}, R.J. Pankhurst^d, C. Galindo^c, J.A. Dahlquist^e, E.G. Baldo^e, C.W. Rapela^f

^a Centro Regional de Investigaciones Científicas y Transferencia Tecnológica de La Rioja (CRILAR-CONICET), Entre Ríos y Mendoza s/n, Anillaco 5301, La Rioja, Argentina

^b INGeReN-CENIIT-UNLaR, Av. Gob. Vernet y Apostol Felipe, 5300 La Rioja, Argentina

^c Dpto. de Petrología y Geoquímica - IGEO (Universidad Complutense, CSIC), 28040 Madrid, Spain

^d British Geological Survey, Keyworth, Nottingham NG12 5GG, United Kingdom

^e CICTERRA-CONICET-UNC, Av. Vélez Sarsfield 1611, Pab. Geol., X5016CGA Córdoba, Argentina

^f CIG-CONICET-UNLP, Calle 1 No. 644, 1900 La Plata, Argentina

ARTICLE INFO

Article history:

Received 22 April 2013

Accepted 9 December 2013

Available online 19 December 2013

Keywords:

I-type magmatism

Middle crust emplacement

Anatexis

Hybridization

Sierra de Famatina

ABSTRACT

A more than 12 km wide sheeted tonalite complex in western Sierra de Famatina, NW Argentina, was emplaced at middle crust levels (ca. 5 kbar), coeval with regional metamorphism during an early phase of the Ordovician Famatinian orogeny (ca. 480 Ma). Advective heat from the tonalite complex caused a rise in the host regional temperatures (≤ 700 °C) by a maximum of ca. 100 °C, developing an aureole (~3 km wide) parallel to the igneous contact. This was accompanied by significant melting (ca. 40%) of the host rocks that hybridized to a variable extent with the tonalitic magmas. Three metamorphic zones were distinguished in a cross-section through the aureole: (1) an external zone consisting of metatextitic gneisses, amphibolites and minor tonalites, (2) an intermediate zone formed by screens of highly melted gneisses, amphibolites and metagabbros lying between tonalite and newly formed leucogranitoid and hybrid rock sheets, and (3) an internal zone formed almost exclusively of massive tonalite and minor hybrid rocks. Incongruent melting of biotite in gneisses of the intermediate zone produced peritectic cordierite and garnet. Hybrids resulting from variable mixing of anatectic granitoids and tonalite magma developed in the innermost part of the aureole at 750–800 °C. Increased water activity within this zone eventually promoted increased melting of plagioclase + quartz in the gneisses. Leucogranitoid magmas formed in part by extraction from the hybrid magmas led to heterogeneity of the Sr-isotope composition. The Cerro Toro contact aureole shows that assimilation of metasedimentary rocks through partial melting can play an important role during emplacement of tonalitic magmas at mid-crustal levels.

© 2013 Elsevier B.V. All rights reserved.

1. Introduction

Thermal aureoles induced by advection of magmas are an excellent natural laboratory for the study of the wall-rock magma interaction processes (e.g., Paterson and Farris, 2008; Paterson et al., 1991 and references therein). Classical examples of thermal aureoles occur when hot magmas intrude upper crustal levels, causing contact metamorphism due to the high thermal contrast between magma and wall-rock. These effects are rather well understood today after long research following the first recognition of contact metamorphism in the late 18th century by James Hutton (e.g., Kerrick, 1970; Pattison and Harte, 1985; Rastall, 1910, among many others). However, mid-crustal thermal aureoles show greater complexity, due to reduced thermal contrast

between magma and the host rocks (which are often affected by pre- or syn-regional metamorphism). In contrast with epizonal contact metamorphism, slow cooling (e.g., Nabelek et al., 2012) permits processes such as assimilation, mingling, mixing and partial melting of the country rocks (e.g., Barnes et al., 2002; Finger and Clemens, 1995; Greenfield et al., 1996; Harris et al., 2003; Jung et al., 1999; Saito et al., 2007; Ugidos and Recio, 1993; Yardley and Barber, 1991). When assimilation occurs its chemical effects are often recognizable, but the physical processes that caused them are less obvious (e.g., Clarke, 2007; Erdmann et al., 2009).

A new example of a contact thermal aureole at mid-crustal level is described from Cerro Toro, in the western Sierra de Famatina (Sierras Pampeanas, NW Argentina, see Fig. 1a). Here, at paleodepths of ca. 17 km, voluminous metaluminous magmas formed a huge sheeted complex (ca. 12 km wide) in predominantly metasedimentary country rocks. A 3-km wide hybridization zone is well displayed along the contact, containing many screens and stoped blocks of host rocks. Although conceptual models of hybridization have recently been well established (e.g., Beard, 2008; Beard et al., 2005), many questions still remain open

* Corresponding author at: Centro Regional de Investigaciones Científicas y Transferencia Tecnológica de La Rioja (CRILAR-CONICET), Entre Ríos y Mendoza s/n, Anillaco 5301, La Rioja, Argentina.

E-mail address: palasino@crilar-conicet.gov.ar (P.H. Alasino).

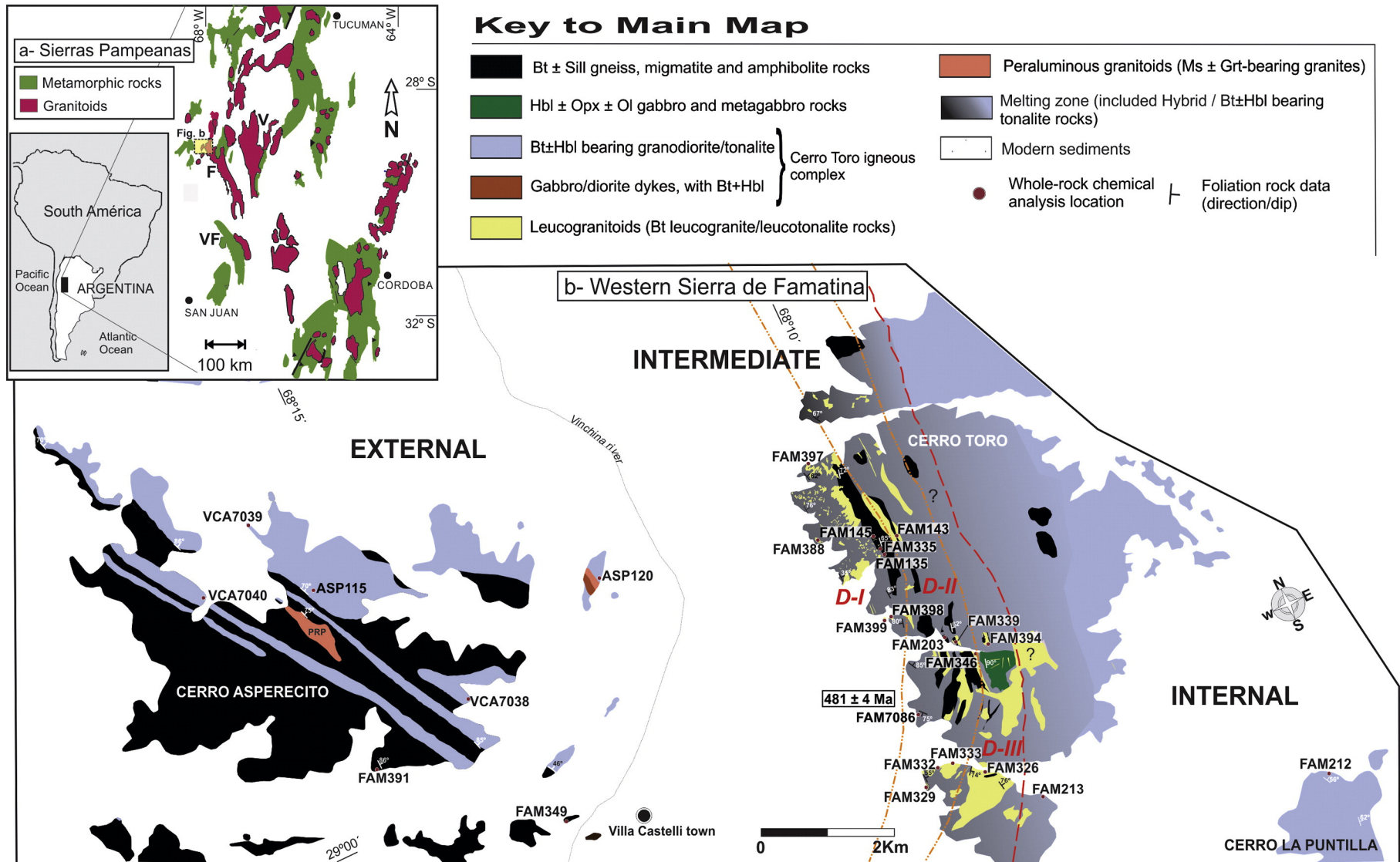


Fig. 1. Simplified geological maps of NW Argentina: (a) Sierras Pampeanas and (b) western Sierra de Famatina. Key for (a): F, Sierra de Famatina; V, Sierra de Velasco; SF, Sierra de Valle Fértil. In (b) from W to E the external, intermediate and internal zones. Limit between external and intermediate zones is not visible, as a reference to this take the Vinchina river. The intermediate and internal zones are limited by a red dashed line, this corresponds to main intrusive contact. In the intermediate zone, the domains I (D-I), II (D-II) and III (D-III) are based on the predominance of specific rock-types: D-I, Bt-Sill ± Crd migmatite blocks; D-II, Bt-Sill ± Grt ± Crd migmatite blocks; and D-III, Bt ± Amp ± Cpx ± Kfs hybrid rocks. PRP Peñón Rosado pluton. Sample FAM175 is outside the mapped area (see Supplementary data). (For interpretation of the references to color in this figure legend, the reader is referred to the web version of this article.)

Table 1
Summary of petrographic characteristics.

General type rock Essential minerals	An% in plagioclase	Biotite type ^a	Accessory mineral
Regional gneisses Quartz > plag > biotite	n.d	n.d	Opq, Fib and Ms*
Regional metatexites Quartz > biotite > plag	14–15	Type-1	Opq, Fib, Ap, Ms*
Diatexite blocks of the intermediate zone Domain I = quartz > plag > biotite > cordierite	15–36	Type-1	Opq, Fib, Ap, Kfs, Ms*
Domain II = quartz > plag > biotite > cordierite > garnet	15–32	Type-2	Opq, Fib, Ap, Kfs, Ms*
Regional tonalites Plag > quartz > biotite > hornblende	48–53	Type-4	Ep, Qpq, Kfs
Hybrid rocks of the intermediate zone Plag > quartz > biotite	core 39–43; rim 33	Type-2	Ep, Opq, Mon, Zrn, Ms*, \pm Amp, \pm Cpx, \pm Kfs
Hybrid rocks of the internal zone Plag > quartz > biotite	core 39–45; rim 24–30	Type-4	Hbl, Ep, Opq, Ap, \pm Kfs
Leucogranite rocks of the intermediate zone Quartz > K-feldspar > plag	11–25	Types-2 and -3	Bt, Ep, Ttn, Ap, Ms*
Leucotonalite rocks of the intermediate zone Plag > quartz > \pm K-feldspar	17–42	Type-2	Bt, Ep, Ttn, Ap, Opq, Ms*

Mineral abbreviations from Kretz (1983). plag = plagioclase. Ms* = secondary muscovite.

^a Types of biotite based on textural and chemical criteria (see text).

concerning natural examples of large-scale interaction between partially molten country-rocks and metaluminous magmas, such as the processes of formation of hybrids and melt extraction during the anatexis. We describe the sheeted intrusions at Cerro Toro, their contact relationships with host-rock screens and stoped blocks, and the partial melting and hybridization processes that occurred in the aureole. We also emphasize the mechanisms that might occur in a regional thermal aureole at mid-crustal level as part of the general construction of magma chambers in orogenic belts.

2. Regional setting

The proto-Andean and subsequent Andean margin of Gondwana has been active from at least the Early Ordovician until the present, which has led to the generation of huge volumes of plutonic and volcanic rocks of different ages. Part of this history is well exposed in the Sierras Pampeanas of NW Argentina (20°–40°S), exposed by tilting of the rigid basement blocks in the Miocene during Andean compression (e.g., Jordan and Allmendinger, 1986). Geochronological data show that four main Paleozoic episodes of granitic magmatism took place in the Sierras Pampeanas: a) Early Cambrian (Pampean orogeny), b) Early–Middle

Ordovician (Famatinian orogeny), c) Middle–Late Devonian (Achalian orogeny) and d) Early Carboniferous. The Famatinian orogeny overprinted the pre-Ordovician terranes along the southwestern Gondwana margin between present Patagonia and Venezuela (Cawood, 2005) and resulted in abundant magmatism in the Sierras Pampeanas (e.g., Pankhurst et al., 1998). The Famatinian Cerro Toro sheeted-complex is found in the western Sierra de Famatina (Fig. 1a), from which the name of the orogeny was derived.

Pankhurst et al. (2000) recognized three distinct Famatinian granitoid-associations in the Sierras Pampeanas: 1) voluminous I-type, 2) more restricted S-type, and 3) minor tonalite-trondhjemite-granodiorite (TTG) type, all emplaced within the interval 484–463 Ma. Detailed petrological, geochemical and isotope studies were carried out by Castro et al. (2013), Dahlquist and Galindo (2004), Dahlquist et al. (2008, 2013), Ducea et al. (2010), Miller and Söllner (2005), Otamendi et al. (2009, 2012), Pankhurst et al. (1998, 2000), Rapela et al. (1990), and Saavedra et al. (1998), among others. I-type intrusions range from gabbro to monzogranite but tonalite and granodiorite are largely dominant. ϵ Nd_t values range from –3 to –9. Only a few Famatinian igneous rocks have positive values of ϵ Nd_t between +0.2 to +4.8 (Casquet et al., 2012; Otamendi et al., 2009, 2012; Pankhurst et al., 2000).

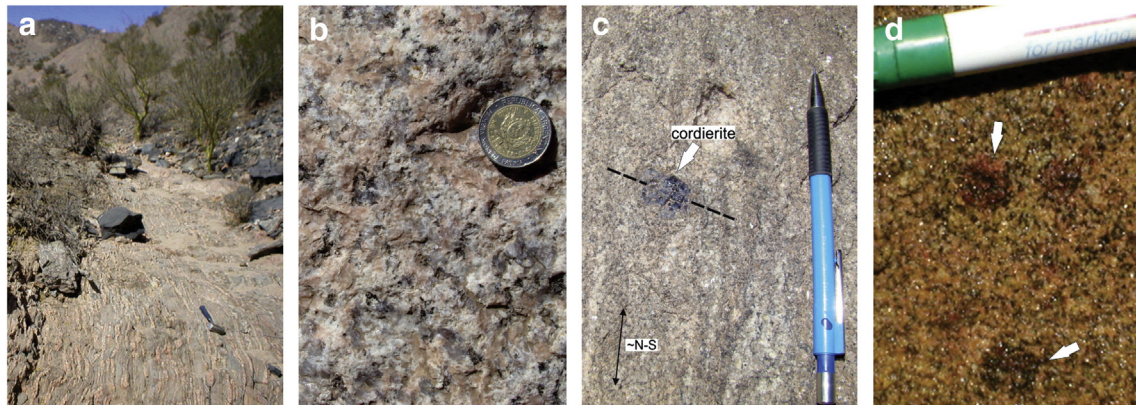


Fig. 2. Field photographs of (a) migmatite rocks from external zone; (b) common texture of leucogranitoids of the intermediate zone; (c) euhedral cordierite (note that it overprints the migmatitic foliation) in migmatites of the intermediate zone; and (d) garnet crystals in a homogenous diatexite of the domain II, intermediate zone.

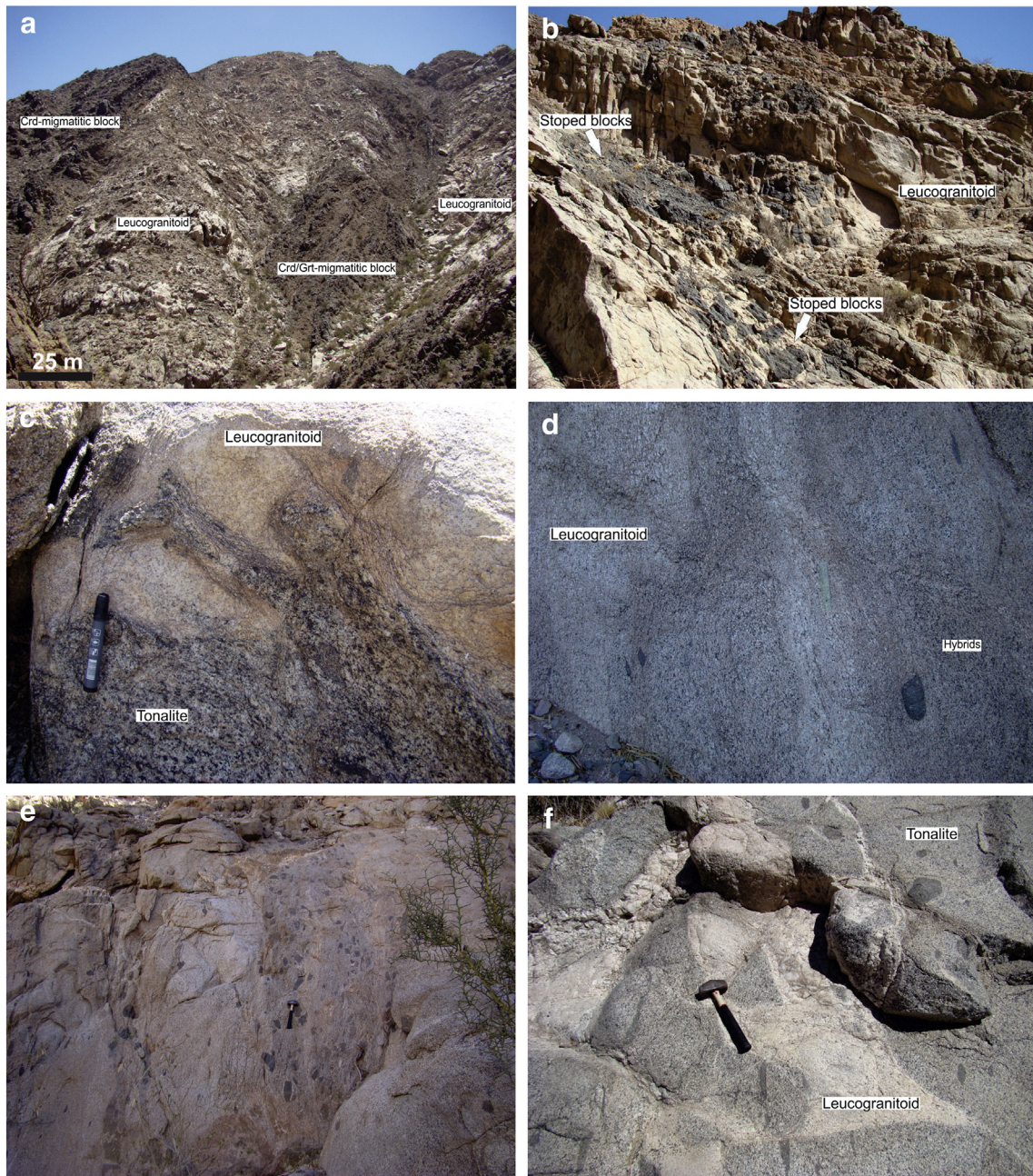


Fig. 3. Intermediate zone: (a) migmatitic blocks of domains I (Crd-bearing) and II (Crd–Grt-bearing) surrounded by leucogranitoid sheeted bodies; (b) dismembering of an amphibolite layer leading to many stoped blocks within leucogranitic magma, partly concordant with the regional structure of the aureole; (c) mingling between the tonalitic unit and leucogranitoids; (d) gradual transition of hybrids to leucogranitoids without signs of retrogression (15 cm ruler for scale); (e) gradual transition of tonalite and hybrid sheets, the latter containing mafic enclaves; and (f) leucogranitoid intruding tonalite at the main intrusive contact (i.e., the boundary between intermediate and internal zones).

3. Sierra de Famatina

The Sierra de Famatina in north-western La Rioja province shows well-exposed sections across the transition from mid-crustal levels in the west (metaluminous basic to intermediate plutonic rocks hosted by gneiss, migmatite, amphibolite and minor meta-basic rocks) to shallow levels in the center and the east (acidic plutonic and volcanic rocks and low- to very low-grade phyllite, metapsammite and chert). Previous geochronological data from the western Sierra de Famatina yielded Early–Middle Ordovician ages (Dahlquist et al., 2008; Pankhurst et al., 2000). We focus here on an area on the western slope of the Sierra de Famatina, near Villa Castelli (Fig. 1a and b). This area is mountainous (up to

2000 masl) and consists from west to east of several sierras: Cerro Aspercito, Cerro Toro, and the northern end of Cerro La Puntilla (Fig. 1b). Here, we recognize the Cerro Toro igneous complex (Saavedra et al., 1992, 1996; Toselli et al., 1988) consisting of a succession of steeply-dipping sheets of tonalite and a large inner pluton that strikes ~N–S and is about 25 km wide (Fig. 1b). The steep dip is probably a primary feature as suggested, for example, by near-vertical strings of stoped blocks within the sheets (see also Castro et al., 2008). Host rocks to the sheets are high-grade metamorphic rocks that display from west to east an increase in grade from amphibolite to granulite facies. Metamorphic rocks are found as screens and stoped blocks within the igneous complex and altogether constitute a medium-P/high-T regional thermal

aureole, i.e., the Cerro Toro thermal aureole. Emplacement at relatively deep crustal levels and under conditions close to anatexis was previously suggested by Saavedra et al. (1992).

4. The Cerro Toro thermal aureole

Three zones can be recognized within the aureole on the basis of field relations, lithology, mineralogy and modal composition. They are well displayed in W–E section: (i) *external*, with high-grade metamorphic rocks, and sheeted bodies of metaluminous igneous rocks (in part of the zone only) and late peraluminous granitoids, (ii) *intermediate*, heterogeneous, with high-grade, partially melted, metamorphic rocks and evidence of widespread hybridization with metaluminous magmas, and (iii) *internal*, consisting mostly of a large tonalite pluton, that extends about 25 km to the east (see Fig. 1b, Table 1 and Supplementary data). Although there is no continuity between the external and the intermediate zones because of disruption by Andean faulting, field relationships and thermobarometry data show that they were parts of the aureole at similar depths. Emplacement of metaluminous magmas and regional metamorphism were largely coeval, which is a distinctive feature of the Famatinian orogeny (e.g., Casquet et al., 2012; Dahlquist et al., 2005; Ducea et al., 2010; Otamendi et al., 2012). U–Pb SHRIMP zircon dating of a hybrid rock from the intermediate zone (FAM7086) has yielded an age of 481 ± 4 Ma with a low zircon εHf_t typical of a

crustal component (Dahlquist et al., 2008, 2013). We consider that this age corresponds to the emplacement of the Cerro Toro complex.

4.1. Description of the zones forming the thermal aureole

4.1.1. External zone

This zone consists mainly of high-grade metamorphic rocks, metatexites with minor intercalations of gneisses, and amphibolites, and is exposed at Cerro Aspercito (Fig. 1b). Foliation is NNW–SSE and dips steeply to the north. Metatexites display a stromatic structure with alternating biotite-rich mesosome, quartz-feldspathic leucosome and biotite and fibrolite-rich melanosome (Fig. 2a). Amphibolites are lens-shaped or tabular and resulted from transposition and metamorphism of former basaltic dykes. On the north-eastern side of Cerro Aspercito (Fig. 1b) metatexites and amphibolites are intercalated with sheets of Bt ± Hbl tonalite and lesser granodiorite of the Cerro Toro igneous complex, largely concordant to the external foliation (sheets, <1 km wide). Most of these bodies show magmatic foliation. Mafic microgranular enclaves, schlieren and xenoliths are common. Mafic intrusions are scarce either as <15 m wide dykes of gabbro-diorite or as small amphibole gabbro bodies. Peraluminous granites (e.g., Peñón Rosado pluton) containing magmatic garnet and muscovite crop out here (Fig. 1b) but they are younger (469 ± 4 Ma, Dahlquist et al., 2007) than the metaluminous intrusions (Fig. 1b).

Intermediate zone												Internal zone	
Mg	Mg	Lgt	Lgt	Lgt	Lgt	Lgt	Lto	Lto	Lto	Lto	Hy	Hy	To
FAM339	FAM335	FAM346	FAM388	FAM394	FAM397	FAM333	FAM326	FAM329	FAM398	FAM399	FAM332	FAM212	FAM213
65.8	66.33	76.31	72.94	77.13	76.97	74.44	71.09	75.13	74.12	77.73	66.55	68.74	62.55
0.78	0.83	0.12	0.21	0.05	0.12	0.2	0.27	0.35	0.367	0.17	0.57	0.38	0.629
17.89	16.05	13.19	14.14	12.24	12.45	14.15	15.85	13.14	13.68	12.78	16.69	15.25	16.99
6.47	6.32	0.97	1.87	0.87	1.32	1.42	2.82	2.83	2.68	1.08	4.63	3.56	5.85
0.12	0.17	0.05	0.04	0.02	0.03	0.05	0.08	0.05	0.03	0.02	0.09	0.08	0.13
2.65	3.03	0.22	0.52	0.05	0.14	0.51	0.63	0.85	0.9	0.55	1.52	1.11	2.25
0.83	0.93	1.63	2.64	0.84	1.54	2.2	3.88	3.41	2.29	1.14	4.19	3.91	5.38
2.15	1.53	3.36	2.66	3.07	3.11	3.13	4.31	2.9	4.49	5.08	3.26	3.02	2.35
3.12	4.73	4.11	4.56	4.98	4.07	3.88	1.02	1.33	1.22	1.76	2.34	2.98	2.07
0.19	0.07	0.04	0.06	0.01	0.02	0.03	0.04	0.02	0.05	0.02	0.17	0.10	0.16
100	99.99	100	99.64	99.26	99.77	100	99.99	100	99.83	100.3	100	99.13	98.36
ppm													
8.39	2.86	2.33	1.4	0.7	1.4	7.58	1.87	4.61	1.3	0.8	6.87	4.5	6.3
149	120	157	90	170	90	119	41.1	69.4	40	50	122	111	112
105	119	60.5	127	15	87	121	171	145	193	112	140	164	217
403	867	340	555	30	695	445	121	97.1	267	166	241	605	406
49.2	51.5	32.5	24.1	12.6	17.9	2.37	17.9	7.11	43	29.5	7.85	45.6	7.99
104	110	69.4	46	24	32	4.29	28.5	11.8	78	51	15.1	89.9	20
11.9	12.4	8.26	nd	nd	nd	0.52	2.86	1.23	nd	nd	1.95	9.48	2.92
44.7	45.8	31.5	20	9	12	1.99	9.36	4.13	36	20	8.53	33.2	14.3
9.32	8.85	7.24	2.44	2.13	1.71	0.63	1.66	0.77	5.12	2.31	2.69	5.95	3.98
1.86	1.67	0.83	0.82	0.31	0.95	0.99	0.86	0.91	1.16	0.7	1.13	1.1	1.11
8.3	6.69	6.91	nd	nd	nd	1.04	1.38	0.65	nd	nd	3.35	4.91	4.32
1.42	0.96	1.18	<0.1	<0.1	<0.1	0.27	0.21	0.1	0.7	0.1	0.54	0.76	0.76
9.13	5.03	7.55	nd	nd	nd	2.18	1.22	0.6	nd	nd	2.98	4.29	4.51
1.98	0.9	1.59	nd	nd	nd	0.53	0.25	0.12	nd	nd	0.57	0.85	0.91
5.78	2.27	4.66	nd	nd	nd	1.67	0.72	0.38	nd	nd	1.49	2.5	2.74
0.92	0.32	0.74	nd	nd	nd	0.28	0.11	0.07	nd	nd	0.21	0.39	0.43
5.89	2	4.91	1.96	1.47	1.29	1.91	0.74	0.56	1.86	0.73	1.38	2.5	2.78
0.94	0.33	0.79	0.29	0.25	0.19	0.33	0.13	0.11	0.29	0.1	0.22	0.37	0.43
7.99	1.91	1.82	0.8	3.2	1	1.17	0.97	1.75	1.4	0.5	0.89	2.01	2.15
17.7	29.9	18.2	3.9	21	5.1	1.97	2.07	1	10.1	2.7	1.62	17.6	1.47
50.1	22.6	41.8	18	10	11	15.4	6.71	3.55	19	6	14.3	23.7	25
15.5	11.6	10.1	nd	nd	nd	4.38	8.08	8.77	nd	nd	15.4	8.8	7.7
155	222	84.2	97	71	118	115	123	96.3	202	108	208	125	167
4.57	6.45	3.25	3.5	3.8	3.2	3.91	3.7	3.29	5.4	4	5.38	3.7	4.5
1.25	0.93	0.6	<0.3	<0.3	0.6	0.83	0.31	0.83	<0.3	0.9	1.6	0.83	0.72
42.2	46.1	28.8	1.01	1.02	1.01	39	28.5	34.9	37.4	47.6	36.9	35.7	40.7
2.24	1.75	1.03	1.40	0.70	1.4	1.07	1.05	1.06	1.07	1.04	1.11	1.01	1.10

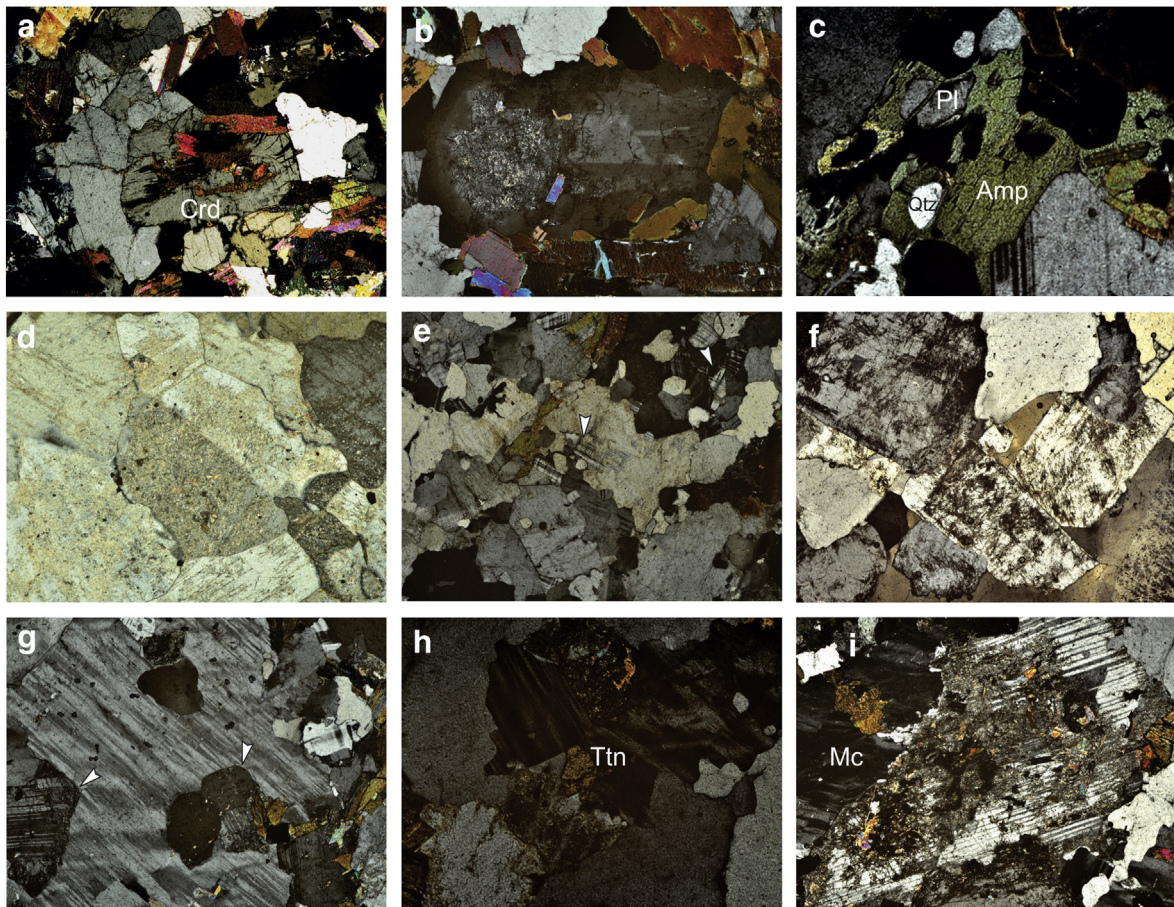


Fig. 5. (a) Euhedral cordierite encloses foliation-forming biotite and fibrolite in a diatextite block of the domain-II, intermediate zone. (b) Hybrid rocks in the intermediate zone showing skeletal plagioclase core surrounded by more albitic rim. (c) Amphibole with rounded inclusions of quartz and plagioclase in a hybrid of the intermediate zone. (d) Monomineralic plagioclase domain in a Bt-leucotonalite of the intermediate zone (specimen FAM398). (e) K-feldspar as interstitial crystals or filling cavities forming micro-veins in partially dissolved plagioclase (Bt-leucotonalite of the intermediate zone, sample FAM399). (f) Leucogranite (FAM397) showing genuine granite texture with euhedral Ab-rich plagioclase. (g) Twinned K-feldspar with unzoned plagioclase showing convex boundaries (sample FAM333). To the left, a partially dissolved pre-existing plagioclase crystal. (h) Titanite associated with K-feldspar in leucogranite (FAM397). (i) Corroded and partially dissolved pre-existing plagioclase contained in anatectic granitoids (sample FAM388). Photo width is 4 mm, except in (c) it is 8 mm. For more information, see text and Table 1.

4.1.2. Intermediate zone

This is located on the western flank of Cerro Toro (Fig. 1b). It is ca. 3 km wide and heterogeneous, displaying a gradual transition from migmatite, through hybrid to leucogranitoid, together with tonalite sheets. Hybrid rocks predominate; they are formed by mixing of the tonalitic magma with partially molten metasedimentary rocks exhibiting a ~N–S sheeted structure. From W to E, they gradually lose the relict metamorphic foliation (defined by biotite) and gradually pass into leucogranitoids. This zone also contains screens and stoped blocks of migmatites, amphibolite and metagabbro up to 3 km long all aligned parallel to the structures in the external zone (Figs. 1b and 3a). Many of these refractory blocks (i.e., amphibolite and metagabbro) are engulfed by leucogranitoids (Fig. 3b), mostly with sharp contacts. Because both screens and blocks resulted from continuous dismemberment at different scales, we will hereafter use block to refer to both. Leucogranitoids in this zone (Table 1 and Fig. 2b) are of two types, (i) leucogranitic or (ii) leucotonalitic. They can be found enveloping migmatite blocks or as concordant or discordant bodies of variable thickness that intruded hybrid and tonalite rocks. Two magmatic foliations can be recognized: ~N–S and W–E. Contacts between all these rocks can be irregular, and gradational or sharp (Fig. 3c, d and e), implying that peak metamorphism, tonalite intrusion and partial melting were almost contemporaneous. Mafic microgranular enclaves, xenoliths and schlieren are common to all these rocks.

On a W–E cross-section through the intermediate zone three domains can be distinguished based on the predominance of specific rock-types (Fig. 1b): (1) domain-I. *Bt–Sill ± Crd migmatites* (Table 1). Migmatite blocks here are diatextites, often with schlieren structures (terms after

Sawyer, 2008) formed by diffuse quartz-feldspar rich bands and thinner and more discontinuous biotite ± cordierite-rich layers, defining a coarse foliation (Fig. 2c). The more homogenous diatextite migmatites are found as patches within and at the outer boundaries of the large migmatitic blocks, the cores of which sometimes exhibit a gneissic texture. (2) Domain-II. *Bt–Sill ± Grt ± Crd migmatites* (Table 1): this domain is defined by the sudden appearance of garnet, together with a modal increase of cordierite in the blocks. Their size decreases significantly (<1.2 km in length) (Fig. 1b). Texturally, migmatites tend to be more homogenous (e.g., FAM143, Fig. 2d). (3) Domain-III. *Bt ± Amp ± Cpx ± Kfs hybrid rocks* (Table 1; Fig. 1b): this is characterized by the predominance of hybrid rocks, leucogranitoids and tonalites. Hybrid rocks commonly show a massive texture but they contain recognizable metamorphic phases (e.g., biotite-2, see Section 6.2). Interpretation of the hybrids as mixtures of partially molten metasedimentary rocks (anatectic melt ± residuum) and tonalitic magma is supported by the low ϵ_{Hf} value (–14.7) of zircon from a sample of this zone (FAM7086, Dahlquist et al., 2013).

4.1.3. Internal zone

This is the easternmost zone and encompasses the eastern flank of Cerro Toro and the northern part of Cerro La Puntilla (Fig. 1b). Here the main rock type is tonalite with a NNW–SSE magmatic foliation defined by orientated biotite and hornblende and containing many mafic microgranular enclaves and some stoped blocks of amphibolite or metagabbro. At the contact with the intermediate zone, leucogranitoids intruded the solidified tonalite front (Fig. 3f). In comparison with

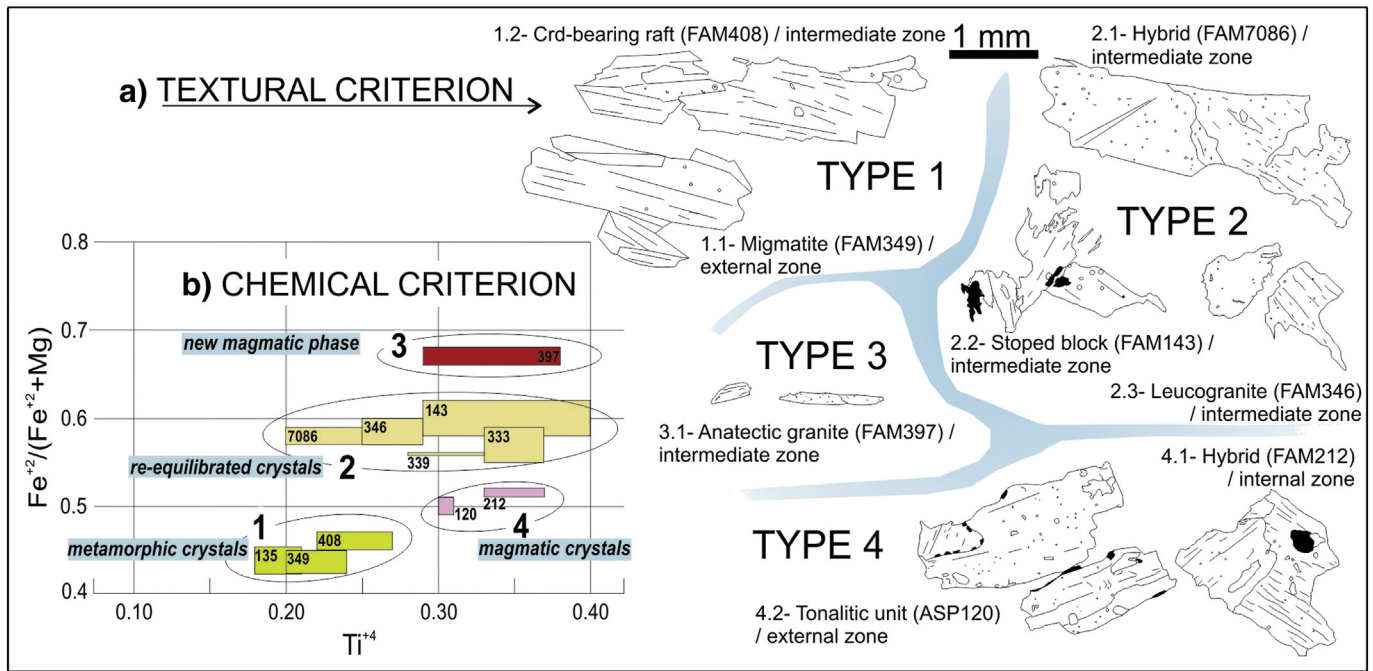


Fig. 6. The four main groups of biotite recognized in the Cerro Toro aureole based on textural (a) and chemical (b) criteria. Type 1, metamorphic biotite; type 2, partially decomposed or re-equilibrated type 1 biotite; type 3, magmatic biotite hosted in leucogranitic magmas; type 4, magmatic biotite belonging to the tonalitic unit. In (a) black corresponds to opaque minerals. In (b) the numbers in boxes correspond to those of analyzed samples. For more information, see Table 1 and Supplementary data.

the hybrids of the intermediate zone with biotite-2, the hybrid rocks here (Table 1) show a greater proportion of tonalite-derived component such as biotite-4 (see Section 6.2) and hornblende. Contact relationships between hybrid and tonalite have not been observed.

In summary, I-type tonalite intrusions were emplaced into heterogeneous rocks (mainly, metasedimentary) affected by coeval regional metamorphism. With increasing proximity to the main tonalite pluton a gradual transition is recognized from metatexitic gneisses (external zone), through diatexite to hybrid and leucogranitoid (intermediate zone). Hybrid and leucogranitic rocks are the result of the interaction between anatectic (\pm solid phases) and I-type magmas. A scheme intended to summarize the relationships between rocks and processes within the aureole is shown in Fig. 4.

5. Analytical methods

Petrographic investigations were conducted on more than 120 representative samples, of which 31 were selected for major and trace element whole-rock analyses using ICP-OES, ICP-MS and/or INAA at ACTLABS, Canada following the procedures described as 4-Lithoresearch and 4E-research codes (methods in www.actlabs.com). Additionally, three representative igneous samples were analyzed by GeoAnalytical Lab, Washington State University, using a ThermoARL sequential X-ray fluorescence spectrometer, following the procedure described by Johnson et al. (1999). All geochemical data are listed in Table 2. Twelve whole-rock analyses published by Dahlquist et al. (2007, 2008) also have been used. Sr and Nd isotope analyses of fourteen representative samples were carried out at the Geochronology and Isotope Geochemistry Center, Complutense University (Madrid, Spain) using an automated multicollector VG® SECTOR 54 mass spectrometer. Errors are quoted throughout as two standard deviations from measured or calculated values. Analytical uncertainties are estimated to be 0.006% for $^{143}\text{Nd}/^{144}\text{Nd}$ and 0.1% $^{147}\text{Sm}/^{144}\text{Nd}$, the latter parameter determined by isotope dilution. Fifty-six analyses of La Jolla Nd-standard over one

year gave a mean $^{143}\text{Nd}/^{144}\text{Nd}$ ratio of 0.511846 ± 0.00003 . Additionally, ten Sr and Nd isotope analyses were taken from Dahlquist and Galindo (2004) and Dahlquist et al. (2008). Mineral compositions were determined using a JEOL Superprobe JXA-8900-M equipped with five crystal spectrometers at the Luis Brú Electron Microscopy Center, Complutense University, Madrid, Spain. Operating conditions were: acceleration voltage 15 kV, probe current 20 nA, and beam diameter 1–2 μm . Absolute abundances for each element were determined by comparison with mineral standards (Jarosewich et al., 1980; McGuire et al., 1992), using an on-line ZAF program.

6. Petrography and mineral chemistry

6.1. Texture and mineral assemblages

6.1.1. Migmatites

Migmatites from the external zone (metatexitic gneisses) consist of Qtz + Pl + Bt₁ \pm Sill (Fib) (Table 1 and Supplementary data) (for the biotite numbers see Section 6.2). As in the intermediate zone, migmatites here show evidence of a melt-phase as suggested by igneous textures such as crystal faces of plagioclase against quartz typical of crystallization from a melt (Vernon, 2004). The mineral assemblage of migmatites from domain I of the intermediate zone is Qtz + Pl + Crd + Bt₁ \pm Sill (Fib) \pm Kfs. That for migmatites in domain II is Qtz + Pl + Crd + Grt + Bt₂ \pm Sill (Fib) \pm Kfs. Cordierite ($0.56 > X_{\text{Mg}} > 0.61$, see Supplementary data), increases from 4 to 11 vol.% on going from domain I to II and occurs either as orientated medium-grained crystals (often altered to muscovite) or large (up to 4 \times 2 cm) prismatic euhedral crystals that include biotite and fibrolite (Fig. 5a). The latter type of cordierite can be found cross-cutting the quartz-feldspathic layers of diatexite (Fig. 2c). Garnet (Alm_{71–74}–Grs_{3–4}–Prp_{10–14}–Sp_{8–16}) only exists in domain II migmatites (up to 3.5 vol.%) and is found as subhedral crystals up to 2.5 cm in size (Fig. 2d). Compositionally, it shows a flat zoning pattern with a slight increase in spessartine content from core to rim (see Supplementary data). Late muscovite is common in both external

Table 3
Summary of thermobarometric results.

1. Sample VCA7009, an amphibolite of the Cerro Aspercito, external zone Holland and Blundy (1994)								
			(Ed–Tr) at 5 kb					T = 694 ± 40 °C
2. Sample FAM143, a Crd–Grt migmatite block of the domain-II, intermediate zone ^a								
Activities and their uncertainties	phl	ann	py	gr	alm	spss	an	
a	0.0194	0.0570	0.00200	4.90e–5	0.320	0.00220	0.430	
sd(a)/a	0.44450	0.34057	0.68750	0.83534	0.15000	0.68112	0.09747	
	ab	crd	fcrd	mncrd	san	ab		
a	0.670	0.330	0.190	0.000680	0.860	0.400		
sd(a)/a	0.05000	0.13467	0.19093	14.70588	0.05000	0.10800		
Independent set of reactions								
	Activity 1 = Sill, H ₂ O, Qtz							
	1) gr + 2sill + q = 3an							
	2) 2py + 4sill + 5q = 3crd							
	3) 2spss + 4sill + 5q = 3mncrd							
	4) 5ann + 6fcrd = 9alm + 5san + 5H ₂ O + 3sill							
	5) 5gr + 3fcrd + 6sill = 2alm + 15an							
	6) phl + 6an = py + 2gr + san + H ₂ O + 3sill							
Results	T = 751 °C, sd = 51,							
	P = 4.6 kbar, sd = 0.7, cor = 0.833, sigfit = 0.61							
3. Sample ASP120, a tonalite of the Cerro Toro complex, external zone								
Holland and Blundy (1994)		Hbl–Pl						T = 746 ± 40 °C
Johnson and Rutherford (1989)		Al–in–Hbl						P = 5.3 ± 0.5 kbar
4. A tonalite of the Cerro Toro complex ^b , intermediate zone								
Johnson and Rutherford (1989)		Al–in–Hbl						P = 5.4 ± 0.5 kbar

^a THERMOCALC software (Powell and Holland, 1988) and the updated version of the ds55 thermodynamic data set (November, 2003; Holland and Powell, 1998). Activity calculated with AX software at 5 kbar and 750 °C.

^b Sample from Saavedra et al. (1996). For mineral chemistry see Supplementary data.

and intermediate zones; it is a retrograde mineral that grew late relative to foliation development.

6.1.2. Tonalites

The typical tonalite consists of plagioclase (An_{48–53}) + quartz + biotite-4 + hornblende, and shows a magmatic hypidiomorphic-granular texture. Close to the boundary with the intermediate zone tonalite of the main pluton exhibits sericitization, and epidotization of plagioclase cores and hornblende, and chloritization of biotite. Secondary epidote can be up to 10 modal %.

6.1.3. Hybrid rocks

Hybrid rocks of the intermediate zone consist of plagioclase + quartz + biotite-2 as essential minerals. Plagioclase exhibits anhedral to subhedral forms with skeletal (box-like-cellular—Fig. 5b) or dusty cores sometimes surrounded by albitic rims (An₃₃). The skeletal plagioclase core is An_{39–43} in composition—intermediate between that of tonalite (An_{49–53}) and metamorphic plagioclase (An_{15–36}). Biotite shows a modal variation (from 20 to 10%, see Supplementary data and Fig. 1b) on going from domain II to III. Clinopyroxene appears as isolated subhedral to euhedral crystals only in domain III. Amphibole occurs either as anhedral crystals including rounded relics of plagioclase, quartz and biotite-2 (Fig. 5c) or replacing clinopyroxene along its boundaries with plagioclase. On the other hand, hybrid from the main pluton (sample FAM212, internal zone) is formed by plagioclase + K-feldspar + quartz + biotite-4 + hornblende. Plagioclase core composition is An_{37–45} surrounded by more albitic rims (An_{24–30}). Hornblende forms subhedral to euhedral crystals.

6.1.4. Leucogranitoids

Leucogranitoids of the intermediate zone range from leucotonalite to leucogranitic (Table 1). Sometimes this modal mineral variation occurs in the same igneous body. Examples of plagioclase-rich rocks (leucotonalite samples FAM326, 398, 399) show variations from a mineral association consisting of anhedral to subhedral plagioclase (An_{17–42}), biotite-2 and recrystallized quartz to one of monomineralic plagioclases, sometimes showing triple points (Fig. 5d). K-feldspar is scarce (<1%) and appears in thin films between recrystallized quartz and plagioclase grains or occupying the volume after partially dissolved plagioclase (Fig. 5e). Conversely, leucogranites (e.g., FAM397) show

typical granitic texture consisting of Ab-rich plagioclase (An_{11–25}, with tabular forms), microcline and biotite-3 (Fig. 5f). K-feldspar is interstitial or forms well defined medium- to coarse-grained crystals. Some rocks (e.g. FAM333, 399) have petrographic characteristics common to both types of leucogranitoids. In thin-section, these rocks exhibit K-feldspar rich zone in contact with monomineralic plagioclase domain, the former consisting of coarse-grained microcline with inclusion of plagioclase (An_{18–33}; crystals devoid of inclusions and with convex boundaries, Fig. 5g). Epidote and titanite can found associated with or included in K-feldspar (Fig. 5h).

Chemical zoning of plagioclase is common in the leucogranitoids. Zoning patterns however are remarkably diverse: (1) An-rich cores (An_{37–43}) surrounded by more albitic rims (An_{26–35}); (2) Ab-rich interiors (An_{18–21}), surrounded by a zone richer in anorthite (An_{30–36}); (3) slightly zoned crystal (An_{27–33}) surrounded by more albitic rims (An_{18–24}) and (4) tabular plagioclase (An_{11–25}) with normal zoning (Fig. 5f). Types 1, 2 and 3 can be recognized in the same thin-section.

6.2. Biotite textural and compositional variation

The petrographic description above of rocks across the aureole shows that biotite is a major phase in all the samples. The chemical composition and texture of biotite characterize the different lithological units in the aureole. Four main groups of biotite have been recognized (Fig. 6 and Supplementary data): (1) Biotite-1 occurs in metatexite migmatites (FAM349) from the external zone, and in Crd-bearing diatexite blocks (FAM135 and 408) corresponding to domain-I (intermediate zone). It is fine to medium-grained, subhedral to anhedral. Common inclusions are monazite, zircon, Ti-magnetite and apatite. Chemically, biotite-1 (n = 20) has X_{Fe} [= Fe/(Fe + Mg)] values between 0.42 and 0.47, intermediate Ti content (from 0.18 to 0.26 a.p.f.u.) and low Mn (from 0.03 to 0.09 a.p.f.u.). Biotite-1 is taken to have formed during regional metamorphism immediately preceding emplacement of the tonalite. (2) Biotite-2 occurs in Grt–Crd bearing diatexite blocks (FAM143 and 339), leucogranitoids (e.g., FAM333 and FAM346) and hybrid granitoids (FAM7086) of intermediate zone domains II and III. Biotite-2 commonly shows inclusion patterns similar to biotite-1. However a marked pleochroism from light to dark brown or even reddish hues, and sometimes rounded shapes are common. Biotite-2 shows higher and more variable values of X_{Fe} (from 0.55 to 0.62), Ti (from 0.20 to 0.40 a.p.f.u.) and Mn

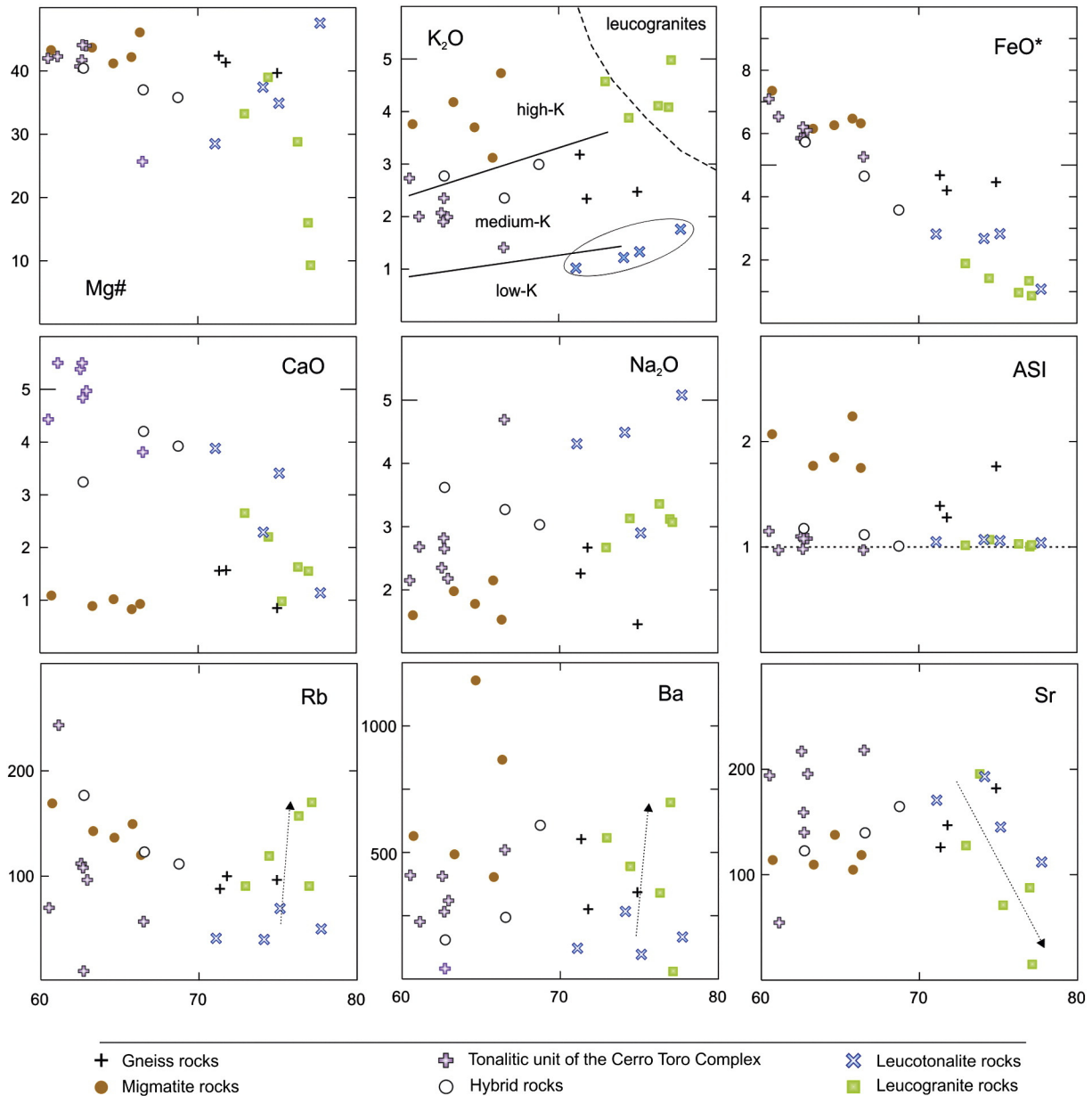


Fig. 7. Whole-rock major and trace element abundances of the Cerro Toro aureole (western Famatina). Mg-number [100*MgO/(MgO + FeO*) molar]. ASI [Al₂O₃/(Na₂O + K₂O + CaO) molar]. K₂O vs SiO₂ diagram with classification boundaries after [Le Maitre et al. \(1989\)](#). For more information, see [Table 1](#).

(from 0.01 to 0.17 a.p.f.u.) (n = 37). Biotite-2 in migmatite reflects increasing metamorphic grade towards the contact with the main igneous body (internal zone). Biotite-2 in leucogranitoid/hybrid rocks is probably a residual mineral from anatexis. (3) Biotite-3 is present in some leucogranitoids of the intermediate zone (FAM397). In contrast biotite-3 is fine-grained, euhedral to subhedral and pleochroic with minor inclusions. It yields high X_{Fe} values between 0.64 and 0.69, and a wide range of Ti contents (0.22 to 0.42 a.p.f.u.) and more restricted Mn (0.06 to 0.12 a.p.f.u.) (n = 8). Biotite-3 commonly occurs as isolated crystals or small clusters suggesting a magmatic origin ([Sawyer, 1999](#)). (4) Biotite-4 is hosted in amphibole-bearing tonalites (ASP120) from the external zone and in hybrid rocks from the internal pluton of the aureole (FAM212). Biotite-4 occurs as medium-grained, euhedral and pleochroic crystals with small inclusions of zircon, monazite and apatite. It has intermediate X_{Fe} values (from 0.49 to 0.52), high Ti (from 0.30 to 0.37 a.p.f.u.) and low Mn (from 0.04 to 0.07 a.p.f.u.) (n = 5) making it easily

distinguishable from the other biotites. Biotite-4 is interpreted as magmatic.

7. Metamorphism

7.1. Prograde mineral reactions

The absence of muscovite as a prograde mineral, which should be expected from the shale/wacke protolith of the migmatites, implies that this mica was consumed in lower-grade metamorphic zones (not visible) by reactions such as $Chl + Ms = Als + Bt + V$ (R1) ([Spear and Cheney, 1989](#)), followed by water saturated reactions of the type $Ms + Pl + Qtz + V = Als + Kfs + melt$ (R2) and $Ms + Pl + Qtz + V = melt$ (R3) [melting reactions (R2) throughout (R5) are from [Spear et al. \(1999\)](#); for P–T conditions see below]. The latter two reactions that consume muscovite and produce (hydrous) melt probably led to the metaxites of the external

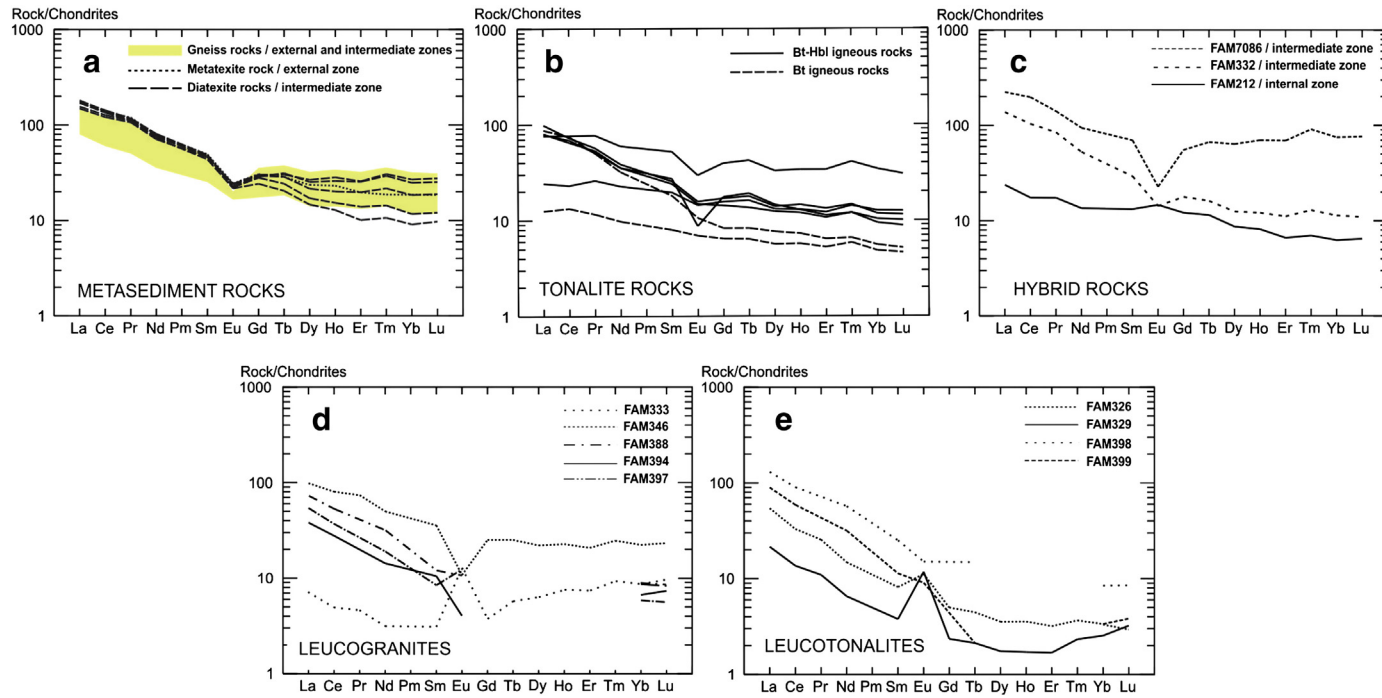


Fig. 8. Chondrite-normalized (after Nakamura, 1974) REE plots of metamorphic and igneous rocks of the Cerro Toro aureole. For more information, see Table 1.

Table 4
Rb–Sr and Sm–Nd data for some metamorphic and igneous rocks of the Cerro Toro aureole, western Sierra de Famatina.

	SiO ₂	Age (Ma)	Rb	Sr	⁸⁶ Rb/ ⁸⁷ Sr	(⁸⁷ Sr/ ⁸⁶ Sr) _{today}	(⁸⁷ Sr/ ⁸⁶ Sr) _t	εSr _(t)	Rock type
<i>Metasedimentary rock</i>									
FAM349	59.25	481	211	106	5.7955	0.752604	0.712885	127	Mg
FAM391	71.77	481	100	147	1.9727	0.731227	0.717707	196	Gg
FAM143	60.72	481	158	119	3.8619	0.74267	0.716202	174	Mg
FAM339	65.80	481	137	115	3.4491	0.742651	0.719012	214	Mg
<i>Regional tonalite, internal zone</i>									
FAM175	66.50	481	58	235	0.7178	0.712539	0.707619	52	To
<i>Hybrid of the intermediate zone</i>									
FAM332	66.55	481	112	123	2.6405	0.730251	0.712154	117	To
<i>Leucogranitoids of the intermediate zone</i>									
FAM333	74.44	481	109	111	2.8546	0.728216	0.708651	67	Lgto
FAM346	76.31	481	150	56	7.7734	0.759402	0.706127	31	Lgto
FAM388	72.94	481	90	127	2.0532	0.722063	0.707991	58	Lgto
FAM394	77.13	481	170	15	33.6395	0.972454	0.741903	540	Lgto
FAM397	76.97	481	90	87	3.0001	0.731954	0.711392	106	Lgto
FAM398	74.12	481	40	193	0.6000	0.713272	0.709160	74	Lto
FAM399	77.73	481	50	112	1.2930	0.718453	0.709591	80	Lto
	SiO ₂	Age (Ma)	Sm	Nd	¹⁴⁷ Sm/ ¹⁴⁴ Nd	(¹⁴³ Sm/ ¹⁴⁴ Nd) _{today}	(¹⁴⁷ Sm/ ¹⁴⁴ Nd) _t	εNd _(t)	T _{DM} [*] (Ga)
<i>Metasedimentary rock</i>									
FAM349	59.25	481	10.01	49.66	0.1218	0.511978	0.511594	−8.3	1.83
FAM391	71.77	481	7.29	39	0.1130	0.512047	0.511691	−6.4	1.70
FAM339	65.80	481	9.32	44.68	0.1261	0.512064	0.511667	−6.9	1.73
<i>Tonalite of the internal zone</i>									
FAM175	66.50	463	10.6	37.6	0.1704	0.512355	0.511818	−3.9	1.51
<i>Hybrid of the intermediate zone</i>									
FAM332	66.55	481	2.69	8.53	0.1906	0.512298	0.511698	−6.3	1.69
<i>Leucogranitoids of the intermediate zone</i>									
FAM333	74.44	481	0.63	1.99	0.1914	0.512183	0.511580	−8.6	1.85
FAM346	76.31	481	7.24	31.46	0.1391	0.512137	0.511698	−6.2	1.69
FAM388	72.94	481	2.44	20	0.0737	0.512053	0.511821	−3.9	1.51
FAM394	77.13	481	2.13	9	0.1431	0.512236	0.511785	−4.6	1.56
FAM397	76.97	481	1.71	12	0.0861	0.512064	0.511792	−4.4	1.55
FAM398	74.12	481	5.12	36	0.0860	0.512088	0.511818	−3.9	1.51
FAM399	77.73	481	2.31	20	0.0698	0.512026	0.511806	−4.1	1.53

The decay constants used in the calculations are the values $\lambda^{87\text{Rb}} = 1.42 \times 10^{-11}$ and $\lambda^{147\text{Sm}} = 6.54 \times 10^{-12} \text{ year}^{-1}$ recommended by the IUGS Subcommittee for Geochronology (Steiger and Jäger, 1977). Epsilon-Sr (εSr) values were calculated relative to a uniform reservoir present day: $(^{86}\text{Rb}/^{87}\text{Sr})_{\text{UR}}^{\text{today}} = 0.0827$; $(^{87}\text{Sr}/^{86}\text{Sr})_{\text{UR}}^{\text{today}} = 0.7045$. Epsilon-Nd (εNd) values were calculated relative to a chondrite present day: $(^{143}\text{Nd}/^{144}\text{Nd})_{\text{CHUR}}^{\text{today}} = 0.512638$; $(^{143}\text{Sm}/^{144}\text{Nd})_{\text{CHUR}}^{\text{today}} = 0.1967$. t = time used for the calculation of the isotopic initial ratios. T_{DM}^{*} = calculated according to De Paolo et al. (1991). For more information, see Supplementary data. Gg, gneiss; Mg, migmatite; Gt, granite; To, tonalite; Lgto, leucogranite; Lto, leucotonalite.

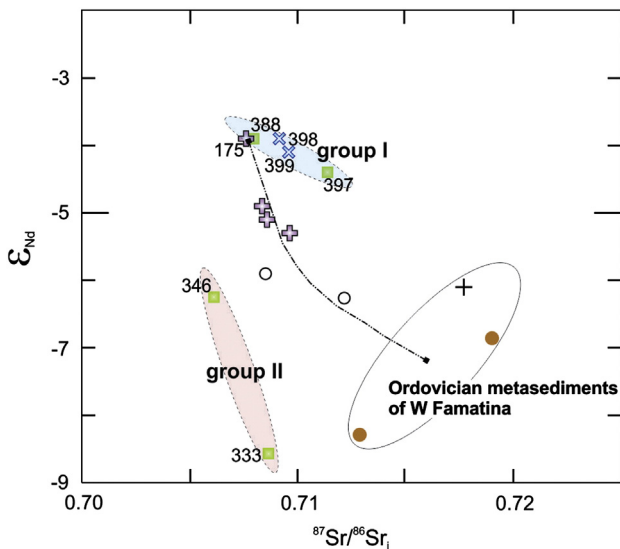


Fig. 9. εNd vs. ⁸⁷Sr/⁸⁶Sr initial plot of metamorphic and igneous rocks from the Cerro Toro aureole. Symbols as in Fig. 7. Four samples (three tonalites = VCA7038, 7039, and 7040 and one hybrid = FAM7086) are from Dahlquist and Galindo (2004). The gray dashed line is a hypothetical simple two-component mixing trajectory.

zone. The modal decrease of biotite and the occurrence of cordierite and garnet with increasing grade (intermediate zone) suggest that biotite dehydration melting also played a role through reactions R4 and R5 (see below). Evidence for melting in the intermediate zone diatexites is provided by textures such as feldspars and cordierite showing crystal faces against quartz, simple twinning in K-feldspar, and aligned euhedral cordierite crystals (e.g., Vernon, 2011). Cordierite encloses foliation-forming biotite and fibrolite (Fig. 5a) implying that the latter minerals were partially dissolved when cordierite formed. Thus, a peritectic origin for most of the cordierite is suggested by means of a reaction of the type: Bt + Sil = Crd + melt ± Kfs (R4) Cordierite and garnet (domain-II of the intermediate zone) formed through the peritectic reaction: Bt + Sil = Grt + Crd + melt ± Kfs (R5).

7.2. Thermobarometry

P–T conditions in metamorphic and igneous rocks from the intermediate and external zones were estimated by means of conventional thermobarometry (Table 3). Sample FAM143 is a Grt–Crd–Bt–Sil–Kfs bearing diatexite block from domain-II of the intermediate zone. P–T conditions for this sample were calculated with THERMOCALC v.3.33 (Powell and Holland, 1988) using the P–T average mode and the updated version of the ds55 thermodynamic dataset (November, 2003; Holland and Powell, 1998). Activity of end members for Grt, Crd, Pl, Bt, and Kfs was computed with the AX software. Selected mineral

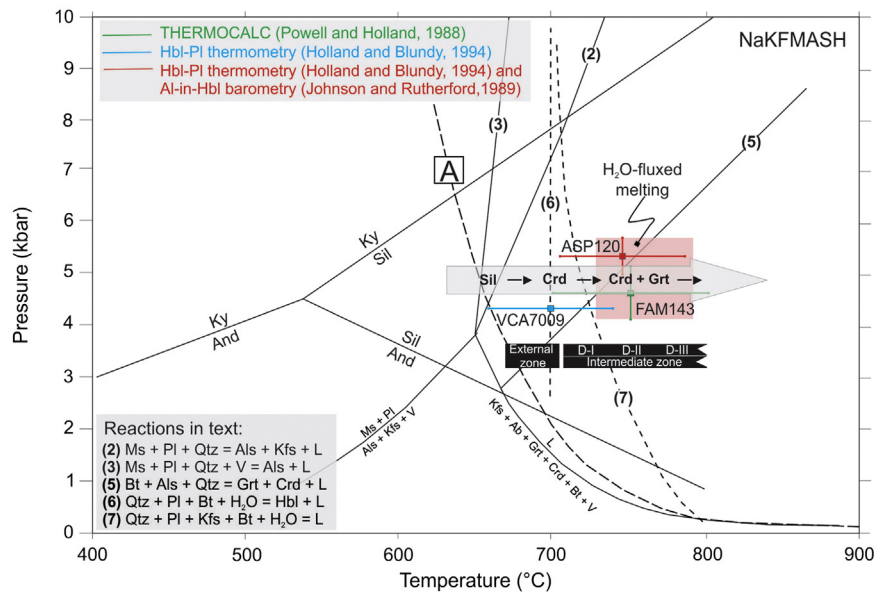


Fig. 10. P–T projection showing thermobarometric results from migmatite (FAM143), amphibolite (VCA7009) and tonalite (ASP120). Metamorphic evolution of the metasedimentary rocks is well explained by reactions 1 through 7 (see text). Reactions 1 and 4 were not included. Reactions 2, 3 and 5 in the NaKMASH system are from Spear et al. (1999). Reactions 6 and 7 are from Büsch (1974) and Peterson and Newton (1989), respectively. The Al_2SiO_5 triple point is from Pattison (1992). The gray arrow indicates nearly isobaric heating path from the external to the innermost intermediate zone of the Cerro Toro aureole.

compositions of garnet, cordierite and plagioclase-cores and biotite-matrix yielded $T = 751 \pm 51$ °C and $P = 4.6 \pm 0.7$ kbar ($\text{cor} = 0.833$, $\text{sigfit} = 0.61$). In the external zone a temperature of 700 ± 40 °C was obtained from an amphibolite (sample VCA7009, Al^{tot} in hornblende = 2.18 ± 0.19 a.p.f.u., $n = 7$) using the Holland and Blundy (1994) Hbl–Pl geothermometer. Estimation of P–T conditions for the emplacement of the Cerro Toro complex was made on hornblende-bearing tonalites. The Holland and Blundy (1994) Hbl–Pl geothermometer and the Al-in hornblende geobarometer (Johnson and Rutherford, 1989) yielded values of $T = 746 \pm 40$ °C and $P = 5.3 \pm 0.5$ kbar for the external zone (ASP-120, Al^{tot} in hornblende = 2.06 a.p.f.u.). The chemical composition of hornblende ($\text{Al}^{\text{tot}} = 2.10$ a.p.f.u.) from tonalite of the intermediate zone (Saavedra et al., 1996) yielded similar values of 5.4 kbar (see Table 3).

In summary, temperature in the aureole ranged from ca. 700 °C in the external zone up to ca. 800 °C in the inner part of the intermediate zone. Pressure was ca. 5 kbar throughout the aureole. These results agree well with location of equilibrium reactions R2 through R5 above (Section 7.1) in P–T projection (Spear et al., 1999).

8. Whole-rock geochemistry

8.1. Major and minor elements

8.1.1. Metasedimentary rocks

Representative whole-rock analyses of metasedimentary rocks are given in Table 2. All the samples show a restricted range of Mg\# [$\text{Mg\#} = 100 \cdot \text{MgO} / (\text{MgO} + \text{FeO}^*)$ molar] between 39 and 46. Within the migmatite group, a representative metatexite from the external zone (FAM349; $\text{SiO}_2 = 59$ wt.%) and diatexites of the intermediate zone (FAM135, 143, 145, 335b and 339; $\text{SiO}_2 = 60$ – 66 wt.%) are similar: $\text{K}_2\text{O} = 3.1$ – 4.9 wt.%; $\text{FeO}^* = 6.2$ – 9.0 wt.%; $\text{Na}_2\text{O} = 1.5$ – 2.2 wt.%; $\text{TiO}_2 < 1.2$ wt.% and $\text{CaO} \leq 1.1$ wt.% (Fig. 7). ASI values range between 1.7 and 2.2. The gneisses of the external and intermediate zone (VCA1004, FAM391 and 203) have SiO_2 contents of 71–75 wt.%, and are dealt with here for comparison only. They show contents of $\text{K}_2\text{O} = 2.3$ – 3.2 wt.%; $\text{Na}_2\text{O} = 1.5$ – 2.7 wt.% and $\text{CaO} = 0.9$ – 1.6 wt.%. In terms of trace elements, Rb content in migmatites is higher than in

the gneisses, whereas Sr content is lower (Fig. 7). REE patterns of the gneisses show La_N/Yb_N ratios between 5 and 8 and weak to moderate negative Eu anomalies ($\text{Eu}_N/\text{Eu}^*_N$ between 0.5 and 0.8) (Fig. 8a). Migmatites show LREE patterns similar to those of the gneisses; HREE however are more variable (Fig. 8a). The migmatites containing garnet (domain-II, intermediate zone) show consistently flatter patterns ($\text{La}_N/\text{Yb}_N = 5.6$ – 7.3) suggesting that HREE were retained in the garnet. Metatexites from the external zone and domain-I diatexites with cordierite and no garnet have steeper patterns ($\text{La}_N/\text{Yb}_N = 9.3$ – 17.2).

8.1.2. Tonalitic unit

The tonalitic unit (samples VCA7038, 7039, 7040, ASP115, 120, FAM213 and 175) does not show major variation in major elements (Fig. 7) with restricted contents of SiO_2 (between 60 and 66 wt.%), CaO (3.8–5.5 wt.%) and alkalis (4.2–6.1 wt.%). Most tonalites plot in the medium-K field on a K_2O vs SiO_2 diagram (Fig. 7). ASI values range from 0.97 to 1.15, i.e., metaluminous to slightly peraluminous. In contrast with major elements, Rb (10–243 ppm), Ba (41–410 ppm) and Sr (54–218 ppm) show significant scatter. The tonalitic unit shows a relative wide range of REE patterns as shown by the variable La_N/Yb_N ratio from 1.9 to 15.7 (Fig. 8b). Bt-tonalite patterns (VCA7038, 7040) do not show

Table 5

Estimates of degrees of partial melting (F) in the Cerro Toro aureole.

	Source	Residue	F
FeO*	4.32	7.35	0.41
MgO	1.65	3.15	0.48
Nb	10.6	16.7	0.33
Sc	16.3	23	0.29
Zn	73	155	0.53
Zr	154	211	0.27
Co	11.8	19.6	0.40
Cr	57.4	91	0.37
			Average 0.38

$F = (C_s - C_r) / C_s$, where C_s is the concentration of an element in the source and C_r is the concentration of the same element but in the residue. Source corresponds to gneisses samples (FAM391 and VCA1004) and the residue to FAM143. Concentrations in wt.% for major elements and ppm for trace elements. Data used in the calculation are available in Table 2.

a Eu anomaly ($\text{Eu}_N/\text{Eu}_N^* = 0.80\text{--}0.97$), while the Hbl-tonalite patterns do ($\text{Eu}_N/\text{Eu}_N^* = 0.40\text{--}0.82$).

8.1.3. Hybrid rocks

The hybrid rocks (FAM212, 332 and 7086, Fig. 1b) show some complexities. They have restricted SiO_2 contents between 63 and 69 wt.%, yield values of Mg# between 36 and 40, and are slightly peraluminous ($\text{ASI} = 1.01\text{--}1.17$). Like other rock types they show a decrease of FeO^* with increasing SiO_2 content (Fig. 7) but no clear trends are displayed on other Harker plots. Some components roughly follow the tonalitic unit trend (e.g., CaO or ASI vs. SiO_2 , Fig. 7), whereas concentrations of other elements are anomalous (e.g., Na_2O or Ba) or can even be compared to those of the migmatites (i.e., K_2O and Rb vs. SiO_2). In the K_2O vs. SiO_2 classification diagram, the hybrid rocks fall close to the boundary between medium- and high-K fields. Chondrite-normalized REE patterns exhibit highly variable La_N/Yb_N ratios from 2.9 to 12.2 and $\text{Eu}_N/\text{Eu}_N^*$ from 0.36 to 1.16 (Fig. 8c). Total REE content varies widely from 48 to 419 ppm.

8.1.4. Leucogranitoids

Regardless of location, leucogranitoids of the intermediate zone show a restricted range of SiO_2 between 71 and 78 wt.% and a clear trend of decreasing FeO^* with increasing SiO_2 (Fig. 7). However the K_2O content allows distinction of two groups that correlate with the petrographic distinction: (i) the leucogranites (FAM333, 346, 388, 394 and 397), with K_2O between 3.88 and 4.98 wt.% that show a wide range of Mg# values (from 9 to 39), and (ii) the leucotonalites (FAM326, 329, 398 and 399) with K_2O between 1.02 and 1.76 wt.% and Mg# values between 28 and 47. Leucotonalites show contents of Na_2O (2.9–5.08 wt.%) and CaO (1.14–3.88 wt.%) higher than in leucogranites ($\text{Na}_2\text{O} = 2.66\text{--}3.36$ wt.% and CaO = 0.84–2.64 wt.%), reflecting quite dissimilar modal proportions of feldspar (see Table 1 and Supplementary data). Moreover, the latter have higher contents of Rb (90–170 ppm) and very variable contents of Ba (30–695 ppm) and Sr (15–127 ppm) compared with leucotonalites: Rb (40–69 ppm), Ba (97–267 ppm) and Sr (112–193 ppm). The average ASI value of leucogranitoids is 1.04 ± 0.02 . In REE patterns the leucogranites reveal a wide range of La_N/Yb_N ratios from 0.8 to 9.3 and $\text{Eu}_N/\text{Eu}_N^*$ from 0.36 to 3.76 (Fig. 8d), whereas the leucotonalites show relatively high LREE but low to intermediate HREE values ($\text{La}_N/\text{Yb}_N = 8.5\text{--}27$) and mostly positive Eu anomalies ($\text{Eu}_N/\text{Eu}_N^* = 1.75\text{--}3.95$) (Fig. 8e).

8.2. Isotope (Sr and Nd) geochemistry

A reference age of 481 Ma for calculation of isotope compositions at the time of metamorphism/magmatism was taken from the weighted U–Pb SHRIMP zircon age of sample FAM7086, a hybrid rock from the intermediate zone (see Fig. 1b) formerly classified as an I-type tonalite by Dahlquist et al. (2008). Migmatites have $^{87}\text{Sr}/^{86}\text{Sr}_{(t)}$ values between 0.7128 and 0.7190 and ϵNd_t values from -6.4 to -8.3 (Table 4). Compared with the published data of three Cerro Toro tonalites ($0.7058 \leq ^{87}\text{Sr}/^{86}\text{Sr}_{(t)} \leq 0.7096$ and $-4.9 \leq \epsilon\text{Nd}_t \leq -5.8$, Dahlquist and Galindo, 2004) the new Hbl-tonalite sample from the tonalite pluton of the internal zone (collected about 20 km to the east of the contact) yields a similar $^{87}\text{Sr}/^{86}\text{Sr}_{(t)}$ value (0.7076) but a higher ϵNd_t (≈ -3.9). Hybrid rocks (FAM332 and FAM7086) yield $^{87}\text{Sr}/^{86}\text{Sr}_{(t)}$ values of 0.7121 and 0.7085, and ϵNd_t values of -5.9 and -6.3 respectively that plot between those of tonalites and migmatites, apparently on an hypothetical two-component mixing line between sample FAM175 (an uncontaminated tonalite; Supplementary data) and the average isotopic composition of the metasedimentary rocks (Fig. 9). A simple calculation with a mixing-equation (Faure, 1986; eq. 9.1, page 141 and Supplementary data) suggests that hybrid rocks could be a mixture of 63% metasedimentary rocks (and/or derived melts) and 37% tonalite magma. Leucogranitoids of the intermediate domain are isotopically heterogeneous; they have $^{87}\text{Sr}/^{86}\text{Sr}_{(t)}$ ratios between 0.7061 and 0.7113, except for sample FAM394 (0.7419), and yield two groups of ϵNd_t values (Fig. 9): most samples (group I; FAM388, 394, 397, 398, 399; Table 4) yield values between -3.9 and -4.6 . Group II (FAM333 and 346; Table 4) with more negative values, -6.2 and -8.6 .

9. Discussion

9.1. Metamorphic evolution of the Cerro Toro aureole

The occurrence of peritectic cordierite and garnet in diatexites of the intermediate zone further suggests that biotite dehydration melting took place. Evidence for anatexis is provided by textures such as feldspars and cordierite showing crystal faces against quartz, simple twinning in K-feldspar, and alignment of euhedral cordierite crystals (e.g., Vernon, 2011). Moreover, some cordierite crystals grew across the foliation, implying that peak-T conditions in the intermediate zone were attained relatively late. Thus, recorded transformations started with

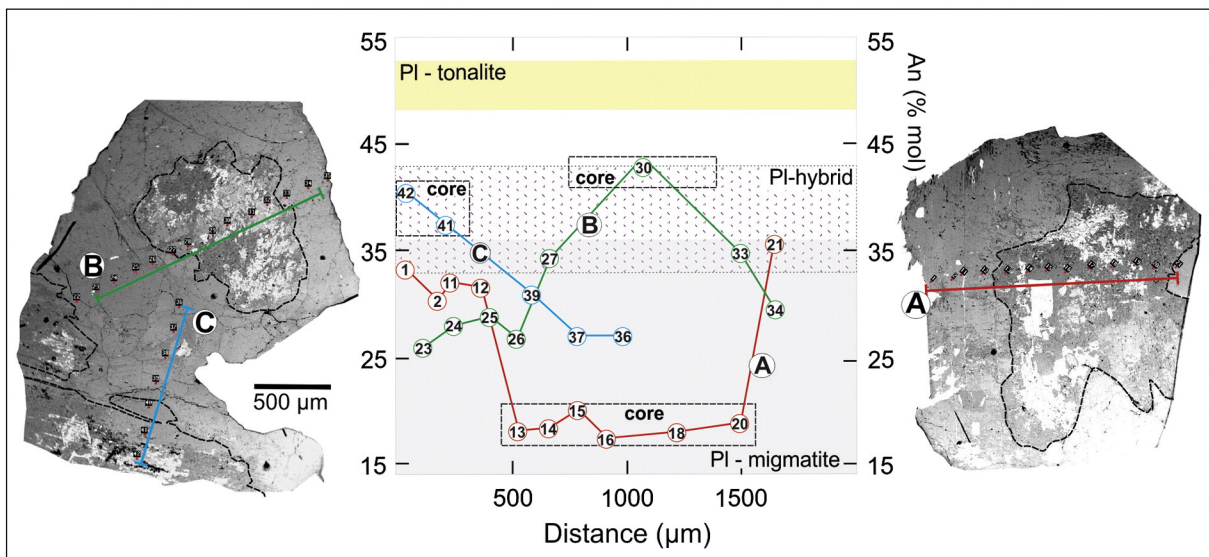


Fig. 11. Back-scattered electron (BSE) images showing the location of electron microprobe spots for plagioclase crystals contained in a leucogranite sample and their corresponding anorthite (An) profiles (A, B and C). An-content of plagioclases from tonalite, hybrid (intermediate zone) and migmatite is also shown. For more information, see Table 1 and Supplementary data.

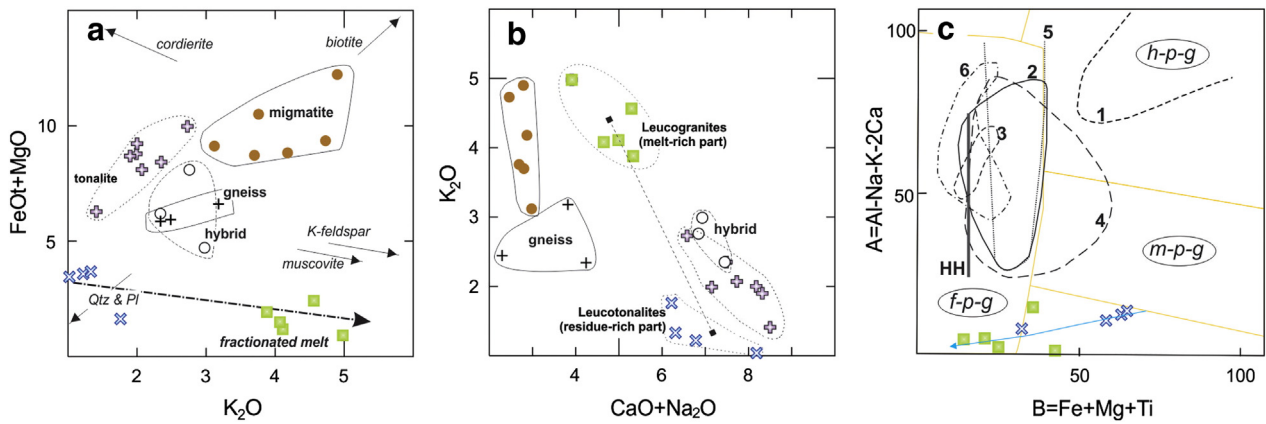


Fig. 12. (a) K₂O versus FeO⁺ + MgO and (b) CaO + Na₂O versus K₂O diagrams showing metasedimentary rocks, hybrids, tonalites and leucogranitoids of the Cerro Toro aureole. In (a) the vectors for K-feldspar, muscovite, quartz + plagioclase and biotite also are shown. (c) A–B diagram after Debon and Le Fort (1983) and Villaseca et al. (1998), showing compositions of experimentally derived melts under water-absent and water-present partial melting at mid-crustal conditions [1, Vielzeuf and Holloway (1988); 2, Holtz and Johannes (1991); 3, Finger and Clemens (1995); 4, Montel and Vielzeuf (1997); 5, Patiño Douce and Johnston (1991); 6, Castro (2004)]. Natural series: HH High Himalaya (Vidal et al., 1982). Fields are: f-p-g (felsic peraluminous granitoids); h-p-g (highly peraluminous granitoids); m-p-g (moderately peraluminous granitoids); and l-p-g (low peraluminous granitoids). Symbols are as in Fig. 7.

the cordierite and garnet-absent assemblage of the external zone at a temperature of ca. 700 °C, followed inwards by domain-I assemblages with cordierite, and these in turn by higher-grade domain-II migmatites with quartz + plagioclase + biotite-2 + cordierite + garnet + K-feldspar + sillimanite at T values of ca. 750 °C (Fig. 10). The geological and petrological evidence above suggests that at Cerro Toro, heat from the tonalite sheeted bodies affected host metamorphic rocks that before intrusion were at temperatures ≤ 700 °C. Advective heating from the

tonalite was responsible for development of a metamorphic aureole with narrow mineral zones parallel to the igneous contact.

9.2. The role of the water in the partial melting of the Cerro Toro aureole

The abundance of anatectic rocks in the intermediate zone (see Fig. 1b) cannot be attributed entirely to biotite-dehydration melting in the temperature range 700–800 °C (e.g., Clemens and Vielzeuf, 1987;

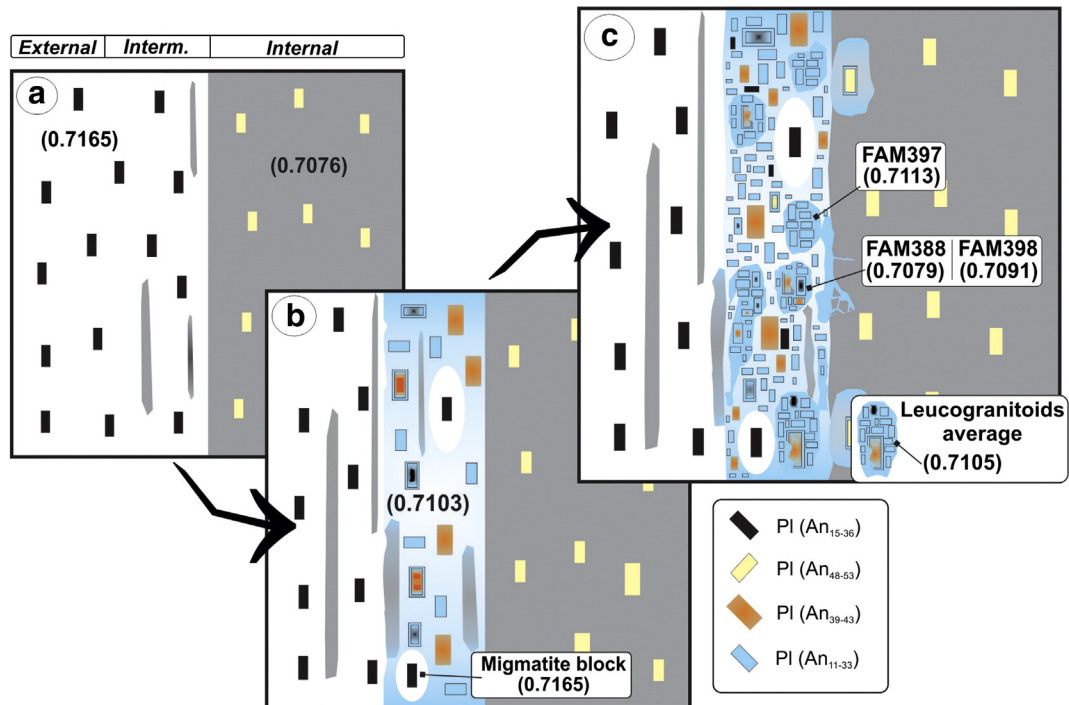


Fig. 13. Model for the formation of isotopic heterogeneities by crystal-melt separation from hybridization zone (after Beard, 2008). (a) Voluminous metaluminous magmas ($^{87}\text{Sr}/^{86}\text{Sr} = 0.7076$) intruded as sheets into partially molten metasedimentary country-rocks ($^{87}\text{Sr}/^{86}\text{Sr} = 0.7165$) under amphibolite facies conditions. (b) Extensive hybridization ($^{87}\text{Sr}/^{86}\text{Sr} = 0.7103$) in the intermediate zone took place. Black and yellow rectangles represent antecrysts from metasedimentary rocks and tonalites (respectively). Antecrysts retain their isotopic features. New plagioclase (orange rectangle) partly composed of country-rock material and partly composed of I-type magmatic material is formed. (c) Variable crystal-melt separation from hybridization zone forming neocrysts (sky-blue rectangles) and crystal overgrowths (sky-blue rims). $^{87}\text{Sr}/^{86}\text{Sr}$ ratios will depend on the proportions of antecrysts and neocrysts. In the figure, numbers in parentheses without denomination of sample represent average of initial $^{87}\text{Sr}/^{86}\text{Sr}$ ratios from Table 4. (For interpretation of the references to color in this figure legend, the reader is referred to the web version of this article.)

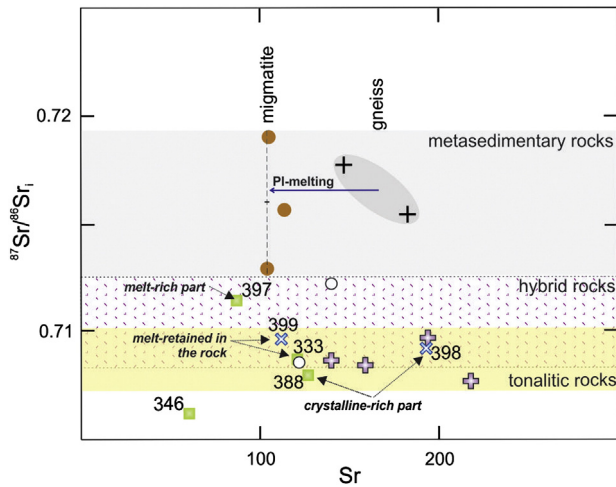


Fig. 14. $^{87}\text{Sr}/^{86}\text{Sr}$ initial versus Sr content of metamorphic and igneous rocks from the Cerro Toro aureole. Four samples (three tonalites = VCA 7038, 7039 and 7040, and one hybrid = FAM7086) were taken from Dahlquist and Galindo (2004). Symbols are as in Fig. 7.

Patiño Douce and Johnston, 1991). This is inferred from the presence of amphibole in the hybrids containing rounded inclusions of plagioclase, quartz and metamorphic biotite-2 (Fig. 5c). This evidence suggests that water-saturated conditions were attained within the aureole to permit reactions such as $\text{Pl} + \text{Qtz} + \text{Bt} + \text{H}_2\text{O} = \text{Hbl} + \text{L}$ (ca. 710 °C at 5 kbar, R6 in Fig. 10). In fact, partial melting experiments on quartz + plagioclase + biotite rocks show that 3–5 wt.% H_2O is required to stabilize amphibole (Conrad et al., 1988; Gardien et al., 2000; Naney, 1983). Moreover, water-fluxed melting consumes more plagioclase than micas since increasing H_2O -activity depresses the $\text{Pl} + \text{Qtz}$ solidus (e.g., Conrad et al., 1988; Patiño Douce and Harris, 1998). Thus, depletion of CaO and Sr in migmatites of the intermediate zone (see Section 8.1.1) could be due to the removal of plagioclase via fluid-enhanced partial melting. On the other hand, amphibole-free hybrid/leucogranitoid rocks in this zone that contain biotite-2 with rounded outlines along with K-feldspar and titanite (see Table 1 and Fig. 5h) indicate hydration melting reactions such as: $\text{Pl} + \text{Qtz} + \text{Bt} + \text{H}_2\text{O} = \text{K-rich melt} + \text{titanite}$ (e.g., Sawyer, 2010) or $\text{Pl} + \text{Qtz} + \text{Bt} + \text{Kfs} + \text{H}_2\text{O} = \text{L}$ (ca. 720 °C at 5 kbar, R7 in Fig. 10). We infer that the intermediate zone migmatites underwent initial metamorphism through mica-dehydration reactions that evolved into wet conditions (water fluxing) near the main tonalite pluton, producing an enhanced zone of extensive melting (Fig. 10). The cause of the inferred water-excess is unknown. However it is at least possible that fluids released deeper in the aureole by means of devolatilization reactions R1 to R4 (Fig. 10) moved up-thermal-gradient and concentrated in the intermediate zone (e.g. Nabelek et al., 2012; Yardley and Long, 1981).

9.3. Estimate of the melt volume in diatexites

According to residue-protolith mass-balance calculations (Sawyer, 1991), if concentrations in the source (C_o), leucosome (C_L) and residue (C_r) are known, an estimate of the degree of partial melting to produce a leucosome can be estimated from the formula $C_o = FC_L + (1 - F)C_r$. However, given the difficulty of recognizing true leucosomes within the aureole, because of the mixing processes described above, an alternative approach is to rely on the source-rock and those elements that are concentrated in the residue (such as FeO^* , MgO, Nb, Sc, Zn, Zr, Co and Cr), when the equation is reduced to $F = (C_r - C_o)/C_r$. The composition of the biotite-rich Grt–Crd diatexite (sample FAM143) was assumed to represent the residue, whereas an average composition of the gneiss samples (FAM391 and VCA1004) was taken as the protolith, based on the recognition of cores with gneissic texture in some migmatitic blocks (see above). The results are shown in Table 5 where it can be seen that

the estimated degree of partial melting in the intermediate zone of the aureole is around 40%. This value seems high, but experimental work with added water (~4 wt.%, required to stabilize amphibole) and temperature about 750 °C yields values similar to this (e.g., Finger and Clemens, 1995; Patiño Douce and Harris, 1998).

9.4. Hybridization and the formation of leucogranitoids

One important issue in the Cerro Toro aureole is the evidence of hybridization in the intermediate zone, resulting from interaction between partially molten migmatite and tonalite magma. Hybrids consist of recognizable metamorphic minerals (e.g., biotite-2) and others, such as skeletal plagioclase, that could be formed (or reequilibrated) after mixing (e.g., Castro, 2001; Erdmann et al., 2007). This plagioclase has a composition intermediate between those of the tonalite and migmatite and experienced temperatures (~750 °C), well above the wet solidus (ca. 690 °C at 6 kbar, Watkins et al., 2007). Moreover, a transition is recognized from these hybrids to leucogranitoids involving progressive loss of metamorphic foliation at the outcrop scale. In fact, the biotite-2 content (ca. 10%) in domain-III hybrids is much lower than in domain-II hybrids (ca. 20%) suggesting that the former involved a higher degree of melting, by means of reactions R6 and R7 above. In turn Bt-poor hybrids gradually pass into massive leucogranitoids; the latter representing a melt-crystal mixture without relics of a metamorphic fabric. Partially resorbed plagioclase cores in leucogranitoids with dissimilar compositions (An_{37-43} and An_{18-21} ; Fig. 11) but with An_{26-36} overgrowths imply that the leucogranitoid magma evolved after the hybrid magma, and that An_{-30} crystallized on inherited plagioclase nuclei (antecrysts).

Leucogranitoid magma differentiated in turn, probably because of magma-mobility enhanced by tectonic deformation within the aureole. Leucotonalites (e.g., FAM326, 398) containing anhedral to subhedral plagioclase (with a wide range of compositions: An_{17-42}) ± biotite-2, together with high contents of Ca, Na and Sr and REE-patterns with Eu-positive anomalies, can be interpreted as a crystalline residuum after the former leucogranitoid magma. Leucogranites (e.g., FAM397) consisting of euhedral plagioclase (An_{11-25}), microcline and biotite-3, with a genuine granitic texture, formed in turn from the residuum-free K-rich magma. They in fact have high contents of K, Rb and REE-patterns with Eu-negative anomalies compatible with this interpretation. Some granitic rocks (e.g., FAM333, 399) with intermediate petrographic characteristics, i.e., equal crystal and melt-rich parts, and with intermediate contents of Ca, Na, K, Rb and Sr, and REE-patterns with a Eu-positive anomaly (see above), probably formed with retention of K-rich melt within the crystalline residuum. Thus, separation of melt from crystals after hybridization may explain the variety of textural and geochemical features shown by leucogranitoids in the intermediate zone of the aureole.

9.4.1. Geochemical constraints: major and trace element compositions

The K_2O vs $\text{FeO}^f + \text{MgO}$ plot (Fig. 12a) helps to distinguish residual ferromagnesian phases from anatexitic melt (e.g., Milord et al., 2001), and clearly shows that the migmatites and gneisses can be described by a combination of quartz + plagioclase and biotite vectors. The contribution of the quartz + plagioclase vector is more marked in gneisses, whereas the biotite vector predominates in migmatites, consistent with the presence of restitic minerals in the latter. Despite the presence of peritectic phases (cordierite or garnet) in the migmatite blocks of the intermediate zone, the latter do not show a trend towards cordierite in Fig. 12a. As for the leucogranitoids, the leucogranites plot along the fractionated melt vector following a clear trend of K_2O -enrichment while the leucotonalites fall near the Qtz + Pl vector (Fig. 12a). These compositional trends may be due to fractional crystallization (e.g., Milord et al., 2001; Sawyer, 1987) yielding a (quartz + plagioclase)-dominated cumulate and a K-feldspar rich fractionated melt. However, the petrographic data above suggest that the leucotonalites do not

correspond to pure magmatic cumulate but to a mixture of residue (dominant) and cumulates. On the K_2O vs $CaO + Na_2O$ diagram (Fig. 12b, incompatible versus compatible elements) leucogranites and leucotonalites define separate fields consistent with melt-rich and residuum-rich rocks derived from anatexis (e.g., Sawyer, 2010). However, both fields are shifted towards higher $CaO + Na_2O$ values compared to the field of the supposed migmatite protolith, i.e., the gneiss. Both are closer to the fields of the hybrids and the tonalites. As in the case of these elements contained in plagioclase, the hybrids show enrichment in Sr but not in Rb when compared with the diatexite rocks (Fig. 7). The diatexites show enrichment in K_2O and lower $CaO + Na_2O$ contents compared to the gneisses, as expected from the increased amount of residual biotite and some K-feldspar after extraction of the anatectic melt.

9.4.2. Leucogranitoids and comparisons with experimental melt compositions

Experimental melt compositions obtained from fertile metasedimentary rock types (e.g., greywacke or pelite) are peraluminous and felsic (Montel and Vielzeuf, 1997; Patiño Douce, 1999). These mostly plot in the field of leucogranite in the A–B diagram (Fig. 12c), often showing a vertical trend similar to those from High Himalayas (e.g., Debon and Le Fort, 1983). When compared with these experimental melt compositions, our leucogranitoids plot partly in the same field (leucogranite) but outside the experimental melt compositions and without a visible vertical trend. They have very low values of A ($= Al-Na-K-2Ca \leq 15$, i.e. a deficit in alumina), indicating a dominant quartzo-feldspathic component. This allows us to hypothesize that our leucogranitoids do not represent pure anatectic crustal melts but involve other components, such as restite minerals and/or mixing with metaluminous-derived liquids (Montel and Vielzeuf, 1997; Patiño Douce, 1999).

9.4.3. Sr–Nd isotope evidence

Major minerals of end-member magmas, i.e., tonalite and anatectic magma, involved in hybridization probably retain their isotopic composition in the hybrid magma (Beard, 2008). In the case of the Cerro Toro aureole, plagioclase controlled the distribution of Sr between the solid and liquid fractions. As explained above, the leucogranitoids contain textural evidence of inherited pre-existing plagioclase crystals (antecrysts), often partially dissolved, suggesting that they formed earlier by crystal–melt separation from hybrid magmas (e.g., Beard, 2008). This explains why the $^{87}Sr/^{86}Sr$ values are lower than those of migmatites (see Section 8.2). Fig. 13 shows a conceptual model for the formation of leucogranitoids. The plot of $^{87}Sr/^{86}Sr$ against Sr (Fig. 14) shows that the leucogranitoids are isotopically intermediate between the migmatites and tonalites. Samples with visible partially dissolved antecrysts (Fig. 5e, g and i) have lower $^{87}Sr/^{86}Sr$ values than antecryst-poor samples (e.g., FAM397–Fig. 5f).

Additionally, solubility of monazite in felsic melts only occurs between 800 and 1400 °C (Montel, 1993). In consequence monazite in the Cerro Toro aureole (T between 700 and 800 °C) was mostly retained in the residual assemblage of migmatites, thus leading to Nd-isotope disequilibrium melting (Watson and Harrison, 1984). In fact, ϵNd values of hybrids and leucogranitoids (group I) less negative than migmatites imply that monazite was not a significant contributor to the Nd budget of these magmas. However group II leucogranitoids with ϵNd values between -6.2 and -8.6 largely retained the Nd isotope composition of the migmatite, i.e., dominated by monazite, while having the $^{87}Sr/^{86}Sr$ composition of tonalites and the petrographic and chemical composition of a leucogranite. These leucogranitoids probably equilibrated with the residual mineralogy (retained or near the source) or incorporated some metamorphic monazite during further injection along the contact with migmatites in the tectonic-enhanced dynamic setting of the aureole. In fact, both samples of this group were collected from leucogranitoids surrounding migmatite blocks. This implies that the magmas either segregated fast and/or that accessories included mostly in biotite-2 were shielded

during water-fluxed melting (e.g., Carrington and Watt, 1995; Jung et al., 1999; Nabelek and Glascock, 1995; Rubie and Brearley, 1990; Zeng et al., 2005).

10. Conclusions

The evidence presented here suggests that the Cerro Toro aureole is a remarkable example of pluton–wall-rock interaction coeval with regional metamorphism and deformation at mid-crustal levels. The main processes involved in the aureole were:

- (1) Sheeted tonalite intrusions were emplaced at the start of the Famatinian orogeny (ca. 480 Ma) into already hot (ca. 700 °C) metamorphic rocks that were separated into screens or disrupted blocks by the tonalite magma. The host rocks were metatexites.
- (2) Increasing temperature within the aureole up to ca. 800 °C at the contact with the main tonalite intrusion triggered mica-dehydration melting reactions in the migmatites, that produced peritectic cordierite followed by cordierite-garnet.
- (3) An increase in water activity probably took place due to hypothetical up-gradient flow of water from deeper in the aureole. The change from “dry” to “wet” conditions triggered the complementary melting of plagioclase + quartz, increasing the amount of anatectic melt in the migmatites up to 40%, and promoting the loss of continuity of the solid mineral framework.
- (4) Hybrid magmas developed by mingling/mixing of tonalite with anatectic magmas in the zone closer to the main tonalite pluton (internal zone). Hybrid rocks show petrographic and geochemical characteristics intermediate between these end-members.
- (5) Variable separation of melt and crystals after hybridization gave rise to leucogranitoid magmas (leucotonalites and leucogranites) that were isotopically heterogeneous, with $^{87}Sr/^{86}Sr$ ratios lower and ϵNd values less negative, respectively, than the migmatites. However, minor leucogranitoids equilibrated with the residual mineralogy or incorporated restitic monazite, resulting in more negative ϵNd values.

Our results suggest that assimilation of country rocks (affected by pre- or syn-regional metamorphism) through partial melting during the emplacement of thick tonalitic magma bodies in the middle crust was an important mechanism in the case of the Cerro Toro aureole. Emplacement in the middle crust favored longer magma-residence time that resulted in effective contamination by assimilation as compared to epizonal intrusions. This supports the idea that the chemistry of Cordilleran magmas does not only reflect their ultimate source characteristics in the subcontinental mantle: they can also undergo prolonged open system magmatic evolution in the middle crust. Under these circumstances, whole-rock isotopic ratios and model ages derived from them must be interpreted with caution.

Acknowledgments

Funds were provided by a Spanish MICINN grant CGL2009-07984/BTE and an Argentinean PICT 1009 grant. We are grateful to S.R. Paterson (USC) for critical review of an earlier draft of this manuscript. P.H. Alasino thanks Carlos Bustamante and Sergio de La Vega for technical support. We thank C.G. Barnes (TTU), J.E. Otamendi (UNRC) and S. Erdmann (UO) for their very constructive reviews that significantly improved the manuscript. We also would like to thank N. Eby (editor) for his comments and suggestions to our manuscript.

Appendix A. Supplementary data

Supplementary data to this article can be found online at <http://dx.doi.org/10.1016/j.lithos.2013.12.006>.

References

- Barnes, C.G., Yoshinobu, A.S., Prestvik, T., Nordgulen, Ø., Karlsson, H.R., Sundvoll, B., 2002. Mafic magma intraplatin: anatexis and hybridization in arc crust, Bindal Batholith, Norway. *Journal of Petrology* 43, 2171–2190.
- Beard, J.S., 2008. Crystal–melt separation and the development of isotopic heterogeneities in hybrid magmas. *Journal of Petrology* 49, 1027–1041.
- Beard, J.S., Ragland, P.C., Crawford, M.L., 2005. Reactive bulk assimilation: a model for crust–mantle mixing in silicic magmas. *Geology* 33, 681–684.
- Büsch, W., Schneider, G., Mehnert, K.R., 1974. Initial melting at grain boundaries part II: melting of rocks of granodioritic, quartzdioritic and tonalitic composition. *Neues Jahrbuch für Mineralogie Abhandlungen* 1974, 345–370.
- Carrington, D.P., Watt, G.R., 1995. A geochemical and experimental study of the role of K-feldspar during water-undersaturated melting of metapelites. *Chemical Geology* 122, 59–76.
- Casquet, C., Rapela, C.W., Pankhurst, R.J., Baldo, E.G., Galindo, C., Fanning, C.M., Dahlquist, J.A., 2012. Fast sediment underplating and essentially coeval juvenile magmatism in the Ordovician margin of Gondwana, Western Sierras Pampeanas, Argentina. *Gondwana Research* 22, 664–673.
- Castro, A., 2001. Plagioclase morphologies in assimilation experiments. Implications for disequilibrium melting in the generation of granodiorite rocks. *Mineralogy and Petrology* 71, 31–49.
- Castro, A., 2004. The source of granites: inferences from the Lewisian complex. *Scottish Journal of Geology* 40, 49–65.
- Castro, A., Martino, R., Vujovich, G., Otamendi, J., Pinotti, L., d'Eramo, F., Tibaldi, A., Viñao, A., 2008. Top-down structures of mafic enclaves within Valle Fértil magmatic complex (Early Ordovician, San Juan, Argentina). *Geologica Acta* 6, 217–229.
- Castro, A., Díaz-Alvarado, J., Fernández, C., 2013. Fractionation and incipient self-granulitization during deep-crust emplacement of Lower Ordovician Valle Fértil batholith at the Gondwana active margin of South America. *Gondwana Research*. <http://dx.doi.org/10.1016/j.gr.2012.08.011>.
- Cawood, P.A., 2005. Terra Australis Orogen: Rodinia breakup and development of the Pacific and Iapetus margins of Gondwana during the Neoproterozoic and Paleozoic. *Earth-Science Reviews* 69, 249–279.
- Clarke, D.B., 2007. Assimilation of xenocrysts in granitic magmas: principles, processes, proxies, and problems. *Canadian Mineralogist* 45, 5–30.
- Clemens, J.D., Vielzeuf, D., 1987. Constraints on melting and magma production in the crust. *Earth and Planetary Science Letters* 86, 287–306.
- Conrad, W.K., Nicholls, I.A., Wall, V.J., 1988. Metaluminous and peraluminous crustal compositions at 10 kb: evidence for the origin of silicic magmas in the Taupo Volcanic Zone, New Zealand, and other occurrences. *Journal of Petrology* 29, 765–803.
- Dahlquist, J.A., Galindo, C., 2004. Geoquímica isotópica de los granitoides de la sierra de Chepes: un modelo geotectónico y termal, implicancias para el orógeno famatiniano. *Revista de la Asociación Geológica Argentina* 59, 57–69.
- Dahlquist, J.A., Rapela, C.W., Baldo, E.G., 2005. Cordierite-bearing S-type granitoids in the Sierra de Chepes (Sierras Pampeanas): petrogenetic implications. *Journal of South American Earth Science* 20, 231–251.
- Dahlquist, J.A., Galindo, C., Pankhurst, R.J., Rapela, C.W., Alasino, P.H., Saavedra, J., Fanning, C.M., 2007. Magmatic evolution of the Peñón Rosado granite: petrogenesis of garnet-bearing granitoids. *Lithos* 95, 177–207.
- Dahlquist, J.A., Pankhurst, R.J., Rapela, C.W., Galindo, C., Alasino, P.H., Fanning, C.M., Saavedra, J., Baldo, E., 2008. New SHRIMP U–Pb data from the Famatina complex: constraining Early–Mid Ordovician Famatinian magmatism in the Sierras Pampeanas, Argentina. *Geologica Acta* 6, 319–333.
- Dahlquist, J.A., Pankhurst, R.J., Gaschnig, R.M., Rapela, C.W., Casquet, C., Alasino, P.H., Galindo, C., Baldo, E.G., 2013. Hf and Nd isotopes in Early Ordovician to Early Carboniferous granites as monitors of crustal growth in the proto-Andean margin of Gondwana. *Gondwana Research*. <http://dx.doi.org/10.1016/j.gr.2012.08.013>.
- De Paolo, D.J., Linn, A.M., Schubert, G., 1991. The continental crustal age distribution: methods of determining mantle separation ages from Sm–Nd isotopic data and application to the Southwestern United States. *Journal of Geophysical Research* 96, 2071–2088.
- Debon, F., Le Fort, P., 1983. A chemical–mineralogical classification of common plutonic rocks and associations. *Transactions of the Royal Society of Edinburgh: Earth Sciences* 73, 135–149.
- Ducea, M.N., Otamendi, J.E., Bergantz, G., Stair, K.M., Valencia, V.A., Gehrels, G.E., 2010. Timing constraints on building an intermediate plutonic arc crustal section: U–Pb zircon geochronology of the Sierra de Valle Fértil–La Huerta, Famatinian arc, Argentina. *Tectonics* 29. <http://dx.doi.org/10.1029/2009TC002615> TC 4002.
- Erdmann, S., London, D., Morgan VI, G.B., Clarke, D.B., 2007. The contamination of granitic magma by metasedimentary country-rock material: an experimental study. *The Canadian Mineralogist* 45, 43–61.
- Erdmann, S., Jamieson, R.A., Michael, A., MacDonald, M.A., 2009. Evaluating the origin of garnet, cordierite, and biotite in granitic rocks: a case study from the South Mountain Batholith, Nova Scotia. *Journal of Petrology* 50, 1477–1503.
- Faure, G., 1986. *Principles of Isotope Geology*, Second edition. John Wiley & Sons.
- Finger, F., Clemens, J.D., 1995. Migmatization and “secondary” granitic magmas: effects of emplacement and crystallization of “primary” granitoids in Southern Bohemia, Austria. *Contributions to Mineralogy and Petrology* 120, 311–326.
- Gardien, V., Thompson, A.B., Ulmer, P., 2000. Melting of biotite + plagioclase + quartz gneisses: the role of H₂O in the stability of amphibole. *Journal of Petrology* 41, 651–666.
- Greenfield, J.E., Clarke, G.L., Bland, M., Clark, D.J., 1996. *In-situ* migmatite and hybrid diatexite at Mt Stafford, central Australia. *Journal of Metamorphic Geology* 14, 413–426.
- Harris, N., McMillan, A., Holness, M., Uken, R., Watkeys, M.K., Rogers, N., Fallick, A., 2003. Melt generation and fluid flow in the thermal aureole of the Bushveld Complex. *Journal of Petrology* 44, 1031–1054.
- Holland, T.J.B., Blundy, J.D., 1994. Non-ideal interactions in calcic amphiboles and their bearing on amphibole–plagioclase thermometry. *Contributions to Mineralogy and Petrology* 116, 433–447.
- Holland, T.J.B., Powell, R., 1998. An internally-consistent thermodynamic dataset for phases of petrological interest. *Journal of Metamorphic Geology* 16, 309–344.
- Holtz, F., Johannes, W., 1991. Genesis of peraluminous granites I. Experimental investigation of melt compositions at 3 and 5 kbar and various H₂O activities. *Journal of Petrology* 32, 935–957.
- Jarosewich, E., Nelen, J.A., Norberg, J.A., 1980. Reference samples for electron microprobe analysis. *Geostandards Newsletter* 4, 43–47.
- Johnson, M.C., Rutherford, M.J., 1989. Experimental calibration of the aluminum-in-hornblende geobarometer with application to Long Valley Caldera (California) volcanic rocks. *Geology* 17, 837–841.
- Johnson, D.M., Hooper, P.R., Conrey, R.M., 1999. XRF analysis of rocks and minerals for major and trace elements on a single low dilution Li-tetraborate fused bead. *Advances in X-ray Analysis* 41, 843–867.
- Jordan, T.E., Allmendinger, R.W., 1986. The Sierras Pampeanas of Argentina: a modern analogue of Rocky Mountain foreland deformation. *American Journal of Sciences* 286, 737–764.
- Jung, S., Hoernes, S., Masberg, P., Hoffer, E., 1999. The petrogenesis of some migmatites and granites (Central Damara Orogen, Namibia): evidence for disequilibrium melting, wall-rock contamination and crystal fractionation. *Journal of Petrology* 40, 1241–1269.
- Kerrick, D.M., 1970. Contact metamorphism in some areas of the Sierra Nevada, California. *Geological Society of America Bulletin* 81, 2913–2938.
- Kretz, R., 1983. Symbols for rock-forming minerals. *American Mineralogist* 68, 277–279.
- Le Maitre, R.W., Bateman, P., Dudek, A., Keller, J., Lameyre, J., Le Bas, M.J., Sabine, P.A., Schmid, R., Sorensen, S., Streckeisen, A., Woolley, A.R., Zanettin, B., 1989. *A Classification of Igneous Rocks and Glossary of Terms*. Blackwell Scientific, Oxford.
- McGuire, A.V., Francis, C.A., Diar, M.D., 1992. Mineral standards for electron microprobe analysis of oxygen. *American Mineralogist* 77, 1087–1091.
- Miller, H., Söllner, F., 2005. The Famatina Complex (NW Argentina): back-docking of an island arc terrane accretion? Early Palaeozoic geodynamics at the western Gondwana margin. In: Vaughan, A.P.M., Leat, P.T., Pankhurst, R.J. (Eds.), *Terrane processes at the margins of Gondwana*. *Journal of the Geological Society of London*, 246, pp. 241–256. Special Publications.
- Milord, I., Sawyer, E.W., Brown, M., 2001. Formation of diatexite migmatites and granite magma during anatexis of metasedimentary rocks: an example from St. Malo, France. *Journal of Petrology* 42, 487–505.
- Montel, J.-M., 1993. A model for monazite/melt equilibrium and the application to the generation of granitic magmas. *Chemical Geology* 110, 127–146.
- Montel, J.M., Vielzeuf, D., 1997. Partial melting of metagreywackes, part II. Compositions of minerals and melts. *Contribution to Mineralogy and Petrology* 128, 176–196.
- Nabelek, P.I., Glascock, M.D., 1995. REE-depleted leucogranites, Black Hills, South Dakota: a consequence of disequilibrium melting of monazite-bearing schists. *Journal of Petrology* 36, 1055–1071.
- Nabelek, P.I., Hofmeister, A., Whittington, A.G., 2012. The influence of temperature-dependent thermal diffusivity on the conductive cooling rates of plutons and temperature–time paths in contact aureoles. *Earth and Planetary Science Letters* 317, 157–164.
- Nakamura, N., 1974. Determination of REE, Ba, Mg, Na and K in carbonaceous and ordinary chondrites. *Geochimica et Cosmochimica Acta* 38, 757–773.
- Naney, M.T., 1983. Phase equilibria of rock-forming ferromagnesian silicates in granites systems. *American Journal of Science* 283, 993–1033.
- Otamendi, J.E., Ducea, M.N., Tibaldi, A.M., Bergantz, G., de la Rosa, J.D., Vujovich, G.I., 2009. Generation of tonalitic and dioritic magmas by coupled partial melting of gabbroic and metasedimentary rocks within the deep crust of the Famatinian magmatic arc, Argentina. *Journal of Petrology* 50, 841–873.
- Otamendi, J.E., Ducea, M.N., Bergantz, W., 2012. Geological, petrological and geochemical evidence for progressive construction of an arc crustal section, Sierra de Valle Fértil, Famatinian Arc, Argentina. *Journal of Petrology* 53, 761–800.
- Pankhurst, R.J., Rapela, C.W., Saavedra, J., Baldo, E., Dahlquist, J., Pascua, I., Fanning, C.M., 1998. The Famatinian magmatic arc in the southern Sierras Pampeanas. In: Pankhurst, R.J., Rapela, C.W. (Eds.), *The proto-Andean margin of Gondwana*. *Geological Society of London, Special Publications*, 142, pp. 343–367.
- Pankhurst, R.J., Rapela, C.W., Fanning, C.M., 2000. Age and origin of coeval TTG, I–S-type granites in the Famatinian belt of NW Argentina. *Transactions of the Royal Society of Edinburgh: Earth Sciences* 91, 151–168.
- Paterson, S., Farris, D., 2008. Downward host rock transport and the formation of rim monoclones during the emplacement of Cordilleran batholiths. *Transactions of the Royal Society of Edinburgh: Earth Sciences* 97, 397–413.
- Paterson, S.R., Vernon, R.H., Fowler, T.K., 1991. Aureole tectonics. *Mineralogical Society of America Reviews in Mineralogy* 23, 673–722.
- Patiño Douce, A.E., 1999. What do experiments tell us about the relative contributions of the crust and mantle to the origin of granitic magmas? In: Castro, A., Fernandez, C., Vigneresse, J. (Eds.), *Understanding granites: integrating new and classical techniques*. *Geological Society, London, Special Publications*, 168, pp. 55–75.
- Patiño Douce, A.E., Harris, N., 1998. Experimental constraints on Himalayan Anatexis. *Journal of Petrology* 39, 689–710.
- Patiño Douce, A.E., Johnston, A.D., 1991. Phase equilibria and melt productivity in the pelitic system: implications for the origin of peraluminous granitoids and aluminous granulites. *Contribution to Mineralogy and Petrology* 107, 202–218.
- Pattison, D.R.M., 1992. Stability of andalusite and sillimanite and the Al₂SiO₅ triple point: constraints from the Ballachulish aureole. *Scottish Journal of Geology* 100, 423–446.
- Pattison, D.R.M., Harte, B., 1985. A petrogenetic grid for pelites in the Ballachulish and other Scottish thermal aureoles. *Journal of the Geological Society of London* 142, 7–28.

- Peterson, J.W., Newton, R.C., 1989. Reversed experiments on biotite-quartz-feldspar melting in the system KFMASH: implications for crustal anatexis. *Journal of Geology* 97, 465–486.
- Powell, R., Holland, T.J.B., 1988. An internally consistent data set with uncertainties and correlations: 3. Applications to geobarometry, worked examples and a computer program. *Journal of Metamorphic Geology* 6, 173–204.
- Rapela, C.W., Toselli, A., Heaman, L., Saavedra, J., 1990. Granite plutonism of the Sierras Pampeanas: an inner cordilleran Paleozoic arc in the Southern Andes. In: Kay, S.M., Rapela, C.W. (Eds.), *Plutonism from Antarctica to Alaska*: Geological Society of America, Special Paper. 241, 241, pp. 77–90.
- Rastall, R.H., 1910. The Skiddaw granite and its metamorphism. *Quarterly Journal of the Geological Society of London* 66, 116–141.
- Rubie, D.C., Brearley, A.J., 1990. A model for rates of disequilibrium melting during metamorphism. In: Ashworth, J.R., Brown, M. (Eds.), *High Temperature Metamorphism and Crustal Anatexis*. Unwin Hyman, London, pp. 57–86.
- Saavedra, J., Pellitero, E., Rossi, J., Toselli, A., 1992. Magmatic evolution of the Cerro Toro granite, a complex Ordovician pluton of Northwestern Argentina. *Journal of South American Earth Science* 5, 21–32.
- Saavedra, J., Toselli, A., Rossi, J., Pellitero, E., 1996. Granitoides y rocas básicas del Cerro Toro. In: Aceñolaza, F.G., Miller, H., Toselli, A.J. (Eds.), *Geología del Sistema de Famatina*. Münchner Geologische Hefte, Reihe A, 19(6), pp. 229–240.
- Saavedra, J., Toselli, A., Rossi, J., Pellitero, E., Durand, F., 1998. The Early Palaeozoic magmatic record of the Famatina System: a review. In: Pankhurst, R.J., Rapela, C.W. (Eds.), *The proto-Andean margin of Gondwana*. *Journal of the Geological Society of London, Special Publication*, 142, pp. 283–295.
- Saito, S., Arima, M., Nakajima, T., 2007. Hybridization of a shallow 'I-type' granitoid pluton and its host migmatite by magma-chamber wall collapse: the Tokuwu Pluton, Central Japan. *Journal of Petrology* 48, 79–111.
- Sawyer, E.W., 1987. The role of partial melting and fractional crystallization in determining discordant migmatite leucosome compositions. *Journal of Petrology* 28, 445–473.
- Sawyer, E.W., 1991. Disequilibrium melting and the rate of melt-residuum separation during migmatization of mafic rocks from the Grenville Front, Quebec. *Journal of Petrology* 32, 701–738.
- Sawyer, E.W., 1999. Criteria for the recognition of partial melting. *Physics and Chemistry of the Earth* 24, 269–279.
- Sawyer, E.W., 2008. *Atlas of Migmatites*, Canadian Mineralogist Special Publication 9. Mineralogical Association of Canada, Quebec, Canada 373 pp.
- Sawyer, E.W., 2010. Migmatites formed by water-fluxed partial melting of a leucogranodiorite protolith: microstructures in the residual rocks and source of the fluid. *Lithos* 116, 273–286.
- Spear, F.S., Cheney, J.T., 1989. A petrogenetic grid for pelitic schists in the system $\text{SiO}_2\text{-Al}_2\text{O}_3\text{-FeO-MgO-K}_2\text{O-H}_2\text{O}$. *Contributions to Mineralogy and Petrology* 101, 149–164.
- Spear, F.S., Matthew, J.K., Cheney, J.T., 1999. *P-T* paths from anatectic pelites. *Contributions to Mineralogy and Petrology* 134, 17–32.
- Steiger, R.H., Jäger, E., 1977. Subcommittee of geochronology: convention on the use of decay constants in geo- and cosmochemistry. *Earth and Planetary Science Letters* 1, 369–371.
- Toselli, A.J., RossideToselli, J.N., Saavedra, J., Pellitero, E., Medina, M.E., 1988. Aspectos Petroológicos y Geoquímicos de los Granitoides del entorno de Villa Castelli, Sierras Pampeanas Occidentales - Sistema de Famatina. *Congreso Geológico Chileno, Actas* 3, 117–128 5°.
- Ugidos, J.M., Recio, C., 1993. Origin of cordierite-bearing granites by assimilation in the Central Iberian Massif (CIM), Spain. *Chemical Geology* 103, 27–43.
- Vernon, R.H., 2004. *A Practical Guide to Rock Microstructure*. Cambridge University Press, Cambridge, UK 594.
- Vernon, R.H., 2011. Microstructures of melt-bearing regional metamorphic rocks. In: van Reenen, D.D., Kramers, J.D., McCourt, S., Perchuk, L.L. (Eds.), *Origin and evolution of Precambrian high-grade gneiss terranes, with special emphasis on the Limpopo Complex of Southern Africa*: Geological Society of America Memoir, 207, pp. 1–11.
- Vidal, P., Cocherie, A., Le Fort, P., 1982. Geochemical investigations of the origin of the Manaslu leucogranite (Himalaya Nepal). *Geochimica et Cosmochimica Acta* 46, 2279–2292.
- Vielzeuf, D., Holloway, J.R., 1988. Experimental determination of the fluid-absent melting relations in the pelitic system. Consequence for crustal differentiation. *Contributions to Mineralogy and Petrology* 98, 257–276.
- Villaseca, C., Barbero, L., Herreros, V., 1998. A re-examination of the typology of peraluminous granite types in intracontinental orogenic belts. *Transactions of the Royal Society of Edinburgh: Earth Sciences* 89, 113–119.
- Watkins, J.M., Clemens, J.D., Treloar, P.J., 2007. Archaean TTGs as sources of younger granitic magmas: melting of sodic metatonalites at 0.6–1.2 GPa. *Contributions to Mineralogy and Petrology* 154, 91–110.
- Watson, E.B., Harrison, T.M., 1984. Accessory minerals and the geochemical evolution of crustal magmatic systems: a summary and prospectus of experimental approaches. *Physics of the Earth and Planetary Interiors* 35, 19–30.
- Yardley, B.W.D., Barber, J.P., 1991. Melting reactions in the Connemara Schists: the role of water infiltration in the formation of amphibolite facies migmatites. *American Mineralogist* 76, 848–856.
- Yardley, B.W.D., Long, C.B., 1981. Contact metamorphism and fluid movement around the Easky adamellite, Ox Mountains, Ireland. *Mineralogical Magazine* 44, 125–131.
- Zeng, L., Saleeby, J.B., Asimow, P., 2005. Nd isotope disequilibrium during crustal anatexis: a record from the Goat Ranch migmatite complex, southern Sierra Nevada batholith, California. *Geology* 33, 53–56.